Nanoscale Advances

ROYAL SOCIETY OF CHEMISTRY

REVIEW

View Article Online
View Journal | View Issue

Cite this: *Nanoscale Adv.*, 2021, **3**, 918

Interface-assisted synthesis: a gateway to effective nanostructure tuning of conducting polymers

Subin Kaladi Chondath and Mini Mol Menamparambath *

The interface-assisted polymerization technique can be viewed as a powerful emerging tool for the synthesis of conducting polymers (CPs) on a large scale. Contrary to other bulk or single-phase polymerization techniques, interface-assisted synthesis strategies offer effective nanostructure control in a confined two-dimensional (2-D) space. This review focuses on the types of interfaces, mechanism at the interface, advantages and future perspectives of the interfacial polymerization in comparison to conventional polymerization techniques. Hence, the primary focus is on briefing the different types of the chemical methods of polymerization, followed by uniqueness in the reaction dynamics of interface polymerization. The classification of interfaces into four types (liquid/solid, gas/liquid, liquid/liquid, and gas/solid) is based on the versatility and underlying mechanistic pathway of the polymerization of each type. The role of interface in tuning the nanostructure of CPs and the performance evaluation of pristine CPs based on the electrical conductivity are also discussed. Finally, the future outlook of this emerging field is discussed and proposed in detail through some multifunctional applications of synthesized conducting polymers.

Received 10th November 2020
Accepted 8th January 2021

DOI: 10.1039/d0na00940g

rsc.li/nanoscale-advances

1. Introduction

In recent years, a substantial amount of research has been executed in the field of conducting polymers. The synthesis, processing and device fabrication of these materials always find a prominent position in the field of material science. Conducting polymers (CPs) can also be classified as organic semiconductors, which can be easily substituted for inorganic conductor materials since they possess some exquisite properties such as the tunable band gap,[1,2] high electrical conductivity,[3–5] provisions for reversible doping/dedoping[6,7] and good biocompatibility.[8,9] Conducting polymers possess a conjugated π-system in their polymer backbone, which enables them to have an intrinsic conductivity that may come around the conductive regime.[10,11] A variety of conducting polymers, such

Department of Chemistry, National Institute of Technology Calicut, Calicut, 673601, Kerala, India. E-mail: neeharabindu@gmail.com; minimol@nitc.ac.in

Subin Kaladi Chondath is currently a PhD candidate in the Department of Chemistry, National Institute of Technology Calicut (NITC). He received his Bachelor's degree in Chemistry (2013) from NSS College, Ottapalam and Master's degree in Chemistry (2015) from Sree Kerala Varma College, Thrissur. His research interests include the synthesis of morphologically tuned polymer-nanomaterial composites for multifunctional applications.

Mini Mol Menamparambath is currently an Assistant Professor in the Department of Chemistry, National Institute of Technology Calicut (NITC). She received her PhD in the optoelectronics of single-walled carbon nanotube composites for flexible electronic applications from Sungkyunkwan University, South Korea in 2014. She is currently focusing on the development of multifunctional nanomaterials using interface-assisted synthesis methods. Her research interests include the synthesis of multi-dimensional nanomaterials, and flexible/stretchable nanomaterial polymer composites for applications, such as energy production and storage, conductive inks and sensors.

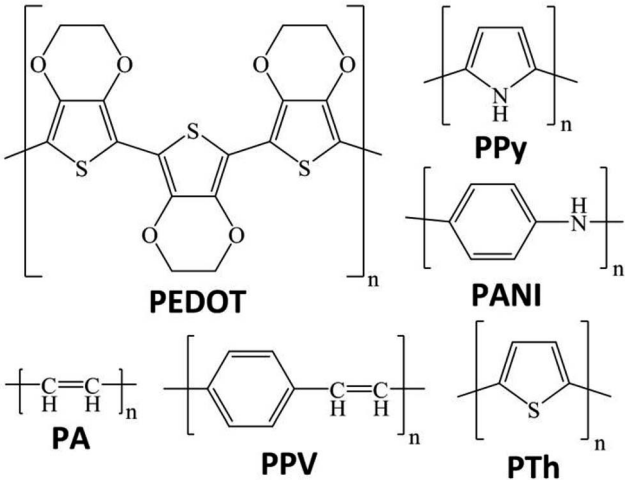

Scheme 1 Chemical structures of some common conducting polymers, such as poly(3,4-ethylenedioxythiophene) (PEDOT), polypyrrole (PPy), polyaniline (PANI), polyacetylene (PA), poly(*p*-phenylenevinylene) (PPV) and polythiophene (PTh).

as polyacetylene (PA), polypyrrole (PPy), polyaniline (PANI), poly(*p*-phenylenevinylene) (PPV), poly(3,4-ethylenedioxythiophene) (PEDOT), and other polythiophene (PTh)-based derivatives, are known to be popularized to date (Scheme 1).[6,8,12–16]

Many chemical and physical synthesis methods have been employed for the effective nanostructure tuning of CPs and its hybrid systems. Some common examples of these methods comprise electrospinning,[5] hard physical template-assisted synthesis,[8] soft chemical template-assisted synthesis (interfacial methods, dilute polymerization, soft template methods *etc.*)[10,17–22] electrochemical methods,[23] and lithography techniques. Each method possesses its own advantages and disadvantages. Considering the depth of the overall synthesis strategies, the major focus is limited only to the chemical methods of polymerization. The ease in synthesis, high reproducibility, high yields and fewer defects in polymer morphologies support the use of chemical methods over hard physical synthesis methods.[8,56,57] The commonly used chemical methods include dilute polymerization, electrochemical polymerization and soft/hard template assisted interfacial synthesis (Fig. 1). These chemical methods are based on bottom-up synthesis protocols, which rely on wet-chemistry synthesis.[56,57] The chemical methods follow an oxidative polymerization pathway, in which the initial nucleation step involves the redox reaction between the monomer and dopant/oxidant/initiator.[20] Typically used dopants are small anions or negatively charged molecules, such as Cl^-,[24] ClO_4^-,[24] and SO_4^{2-}.[10] Larger anions, such as PSS (polystyrene sulfonate anion)[25,26] and even DNA, were reported as effective dopants in polymer synthesis.[27] Dopants not only initiate the polymerization, but also affect the physical and chemical properties of the obtained polymer.[24] A typical dilute polymerization is a one-pot synthesis method, which comprises a monomer and one or more oxidants dissolved or dispersed in a common solvent (Fig. 1a.1).[28,29] Most of the monomer precursors are soluble in water, and water is usually opted as a common solvent. The inherent nature of the polymer decides the end morphology unless no external foreign agents are introduced into the system. These foreign agents may be soft shape directing templates like surfactants (methyl orange,[30–32] PVP,[33,34] SDS,[35] CTAB[35]) (Fig. 1a.2) or even UV photons.[22,36–39] Interfaces can be viewed as a soft template for the effective CP nanostructure tuning through the organization of reactive molecules (Fig. 1a.2).[56,57] The CP films were mainly synthesized by electrochemical routes, which functions through a three-electrode setup containing a monomer solution and dopants.[9,38,40] Here, the dopant functions as both supporting electrolyte and source of dopant anion for the electrochemical polymerization (Fig. 1a.3). Hard templates, such as porous alumina film,[8,26,41,42] zeolites[15,28,43,44] and anodic aluminum oxide,[6,12] were also proved successful for the effective nanostructure tuning of CPs (Fig. 1a.4). However, the complex removal steps restrict them to use as structure guiding agents in dilute polymerization systems.[8] Agglomerates of PANI nanofibers were reported in a single solvent dilute polymerization setup using ammonium persulfate (APS) as the oxidant.[28,43] Similarly agglomerated spheres of PPy and its composites were synthesized in an aqueous medium, along with suitable oxidants.[45,46] The 3-D rambutan-like PANI spheres were prepared by the use of perfluorooctane sulfonic acid (PFOSA).[47] Perfluorosebacic acid (PFOSA) was recognized both as a dopant and template for the self-assembly process of PANI nanofibers for the formation of dandelion-like microspheres.[48] Interface-assisted methods provide room for the synthesis of high aspect ratio polymer nanostructures (tubes, wires and films) of high dimensions (1-D and 2-D).[10,20,56,57] Electrochemical polymerization serves as the most ideal method for the synthesis of CP films with good yield and electronic properties.[38,49] One-dimensional (1-D) CP nanostructures with high aspect ratios are widely synthesized using hard templates, such as porous alumina film, zeolites and anodic aluminum oxide. Growing the CP tubes or wires inside the pores or channels of these membranes is a widely accepted synthesis strategy.[26,41,42]

The dilute polymerization and electrochemical routes were well explored in many years. However, the diverse nanostructure tuning of CPs for multifunctional applications was still a tricky problem for these methods. The unimaginable properties of interfaces for the effective CP nanostructure tuning were intriguing and untouched by scientists for the past few decades. To overcome the disadvantages possessed by the single solvent-based chemical methods (dilute polymerization and electrochemical routes), interface-assisted polymerization techniques emerged as a promising bottom-up synthesis strategy.[56,57] The interface can act as either a soft template or removal hard template for the effective nanostructure control of CPs by controlled diffusion and regulated orientation of monomers. The major types of interfaces are liquid/solid (L/S), gas/liquid (G/L), liquid/liquid (L/L) and gas/solid (G/S). These interfaces offer room for the synthesis of a wide variety of materials, such as carbon sheets,[50] metal oxide sheets,[51] transition metal dichalcogenides,[51] and two-dimensional CPs (2-D CPs). For example, chemical vapor deposition (CVD)[52,53] is

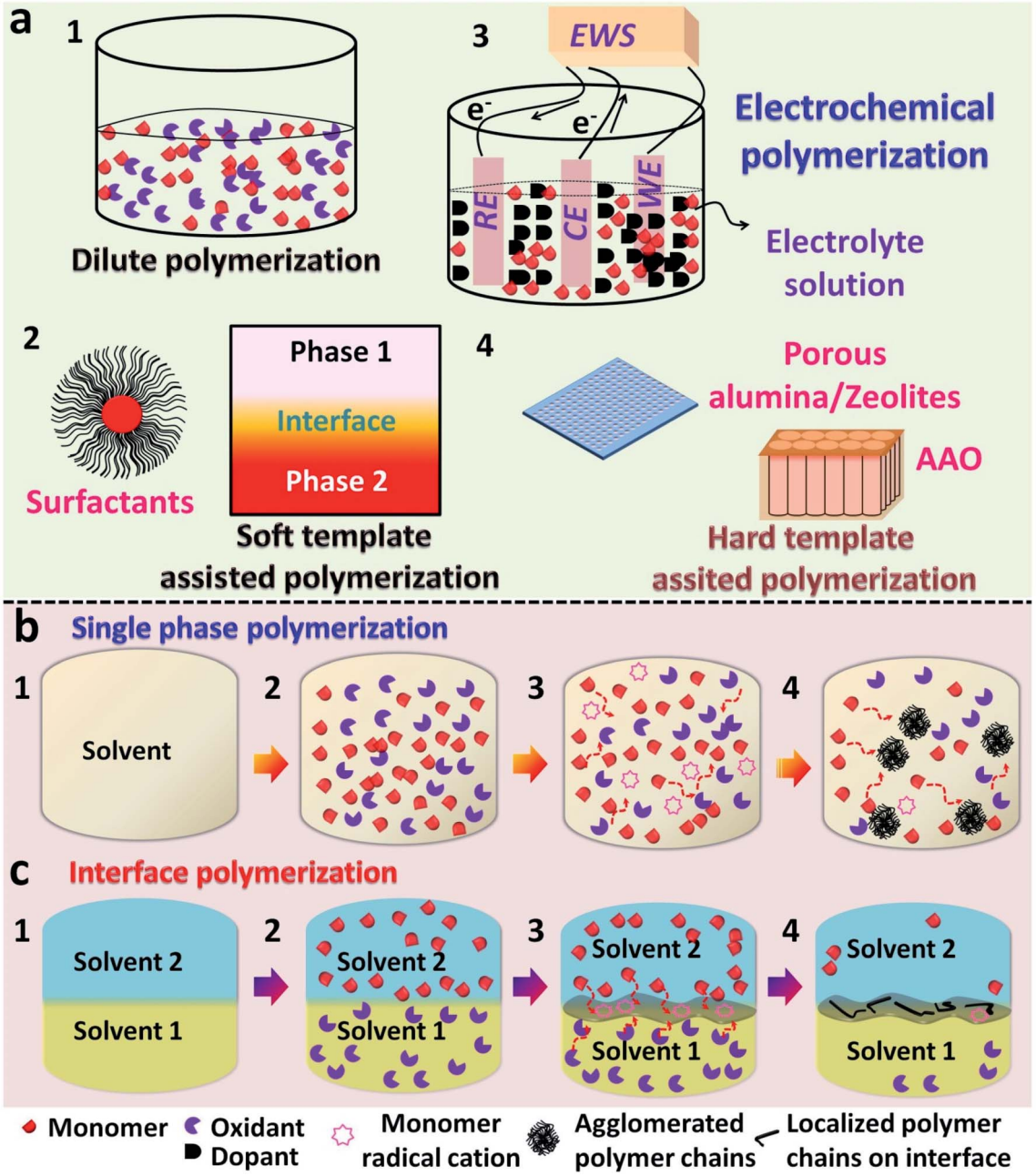

Fig. 1 (a) Schematic illustration of the commonly used polymerization methods: (1) dilute polymerization, in which the monomer and oxidant are both dissolved in a single solvent, accounts for the polymerization, (2) soft template-assisted polymerization, in which the surfactants and interfaces tune the morphology/rate of polymerization, (3) electrochemical polymerization, in which the three-electrode setup of the reference electrode (RE), counter electrode (CE) and working electrode connected to an electrochemical workstation (EWS) immersed in electrolyte solution results in the polymerization in a single-phase system, and (4) hard template-assisted polymerization tuned by porous alumina, zeolites and anodic aluminum oxide (AAO). Schematic illustration of (b) single phase and (c) interface polymerization mechanisms, in which 1 to 4 represent the various steps of each polymerization mechanism. Curved arrows represent the random/directed motion of the reactants at the single phase and interfacial systems. Single phase polymerization starts with the following: (1) a suitable solvent is taken in a reaction vessel, (2) monomer and oxidant molecules are dispersed in the solvent, (3) the initiation of the polymerization reaction, in which the redox reaction between monomer and oxidant molecules results in to the formation of monomer radical cations (the three dimensional diffusion of monomer and oxidant molecules in the same solvent is indicated in the form of red colored curved arrows), and (4) the subsequent polymerization steps followed by secondary growth of oligomer chains attributed to the formation of agglomerated nanostructures. Interface polymerization starts with the following: (1) two immiscible solvents were taken in a reaction vessel, (2) monomer and oxidant molecules were dispersed in the corresponding solvents, (3) formation of a distinguishable interface between two immiscible solvents, followed by the formation of monomer radical cations delocalized at the interface through the redox reaction between monomer and oxidant molecules (the directed diffusion of monomer and oxidant molecules towards the interface is represented in the form of red curved arrows), and (4) localization of polymer chains at the interface due to the high interfacial tension.

a classic example for a G/S-assisted interfacial polymerization, in which a metal or carbon offers a hard 2-D template for the adsorption, nucleation, arrangement and polymerization of corresponding precursors or intermediates (carbon radicals from CH_4 for graphene synthesis). Thus, the solid surface acts as a template for the controlled polymerization of monomers. The underlying mechanism behind every interfacial polymerization technique is the preferable orientation of monomers or precursors above the reactive interface.[20,56,57] This review article enlightens the recent trends in various interface-assisted polymerization techniques for the nanostructure tuning of CPs and its hybrid systems. The review starts with the overview of interface-assisted synthesis, including the chemistry, mechanism and various types. After that, a detailed description consisting of the current efforts in interfacial polymerization methods will be summarized in detail with the help of recent literature examples. The role of the diverse interactions at the interfaces in tuning the nanostructure of conducting polymers and a detailed comparison between various synthesis strategies were made on the basis of the electrical conductivity of CPs. The major future outlook of the review has also been summarized through some of the potential applications of the CP based systems. The concluding section gives an outline of the capabilities of the interface-assisted techniques in CP nanostructure tuning, especially for the synthesis of 2-D CP sheets/films. The reports published in the last decade were analyzed in order to classify the various types of interfacial polymerization methods on the basis of synthesis methodologies. Herein, we aim to provide a succinct summary of various interface-assisted polymerization techniques that may provide a strong basis for subsequent investigation in this emerging field of interface-assisted polymerization. This review article will provide a brief idea about the tremendous possibilities of various interface-assisted polymerization techniques for the synthesis of CP based systems for multifunctional applications.

2. Uniqueness in the reaction dynamics at the interface

An interface is a curved or flat surface between two different phases (can be viewed as a phase boundary) possessing a thickness ranging from several angstroms to even micrometers in size.[20,56,57] It can be also considered as an imaginary membrane initiating the selective flow of matter between two immiscible phases.[20] The interfacial polymerization was proved to direct the polymerization to yield high molecular weight polymers, like polyamides, polyesters and polyurethanes, which were synthesized previously through conventional single phase methods.[54,55] The synthesis of conducting polymers involves chemical oxidation polymerization (COP) through the redox reaction between monomers and oxidant, and the inherent properties of CPs are largely influenced by the type of nanostructures. The constant need of high aspect ratio CP nanostructures (tubes, wires, sheets and flowers) paved the way for the utilization of interface-assisted techniques as an effective tool. The interface is well known to direct polymerizations through the self-assembly and nucleation of monomers by selective transport of monomers and reactants towards it.[20,56,57] Due to the unbalanced forces, reactions at the interfaces are entirely different from that of a homogenous, single phase, reaction mixture.[20] In a single phase polymerization setup, all of the reactive components are in the same phase, and the secondary growth of the oligomers takes place through the three-dimensional diffusion of monomers. The resultant morphology will be restricted to agglomerated ones with limited properties (Fig. 1b). A typical interface-assisted polymerization involves a system of immiscible phases, along with the distribution of monomers/reactants in the respective phases. Unlike a single-phase polymerization setup (dilute polymerization and electrochemical routes), an interfacial polymerization reaction between monomers and reactants are triggered in slow, controlled rates by the selective diffusion of monomers towards the interface.[20,56] The high interfacial tension between two immiscible phases acts as a driving force for the migration of nanosized particles towards it.[10,20] This leads to the anchoring of monomers at the interface, leading to the controlled growth of polymer chains (Fig. 1c). Since the polymer chains are isolated from the unreacted monomers/oxidants, the secondary growth is inhibited and the end morphology will be extended towards high aspect ratio ones (tubes, wires, sheets and films). The stabilization of the interfaces through the selective adsorption of inorganic silicon oxide nanoparticles in an oil-in-water pickering emulsion was reported by Chevalier *et al.*[58] Gold nanoparticles were found to be delocalized on a water/dichloroethane (water/DCE) interface under the influence of interfacial tension stabilization.[59] A sequential decrease in the interfacial energy was measured at the water/DCE. The superiority of the interface-assisted techniques in effective nanostructure control over the conventional single-phase methods is encouraging for the materials scientists to discover tremendous possibilities in CP synthesis. The theoretical models of the polymerizations predict the growth rate and thickness of the CPs by regulating the polymerization time. The simulated model proposed by Ji and coworkers[60a,b] establishes the relationship between the polymerization time (t) and thickness (X) of the thin polymer film in a L/S interfacial system, as shown in eqn (1).

$$t = -((E_0/B_0) + ((A_0D_0)/B_0^2) + ((C_0A_0^2) + B_0^3))\ln(1 - (X/X_{max})) - (C_0/2B_0)X^2 - ((D_0/B_0) + (C_0A_0)/B_0^2) \quad (1)$$

where A_0, B_0, C_0, D_0, and E_0 are the constants derived from the diffusion coefficient, reaction rate, concentration of the monomers, and the parameters of the solid substrate, and X_{max} corresponds to the maximum value of X when the polymerization time reaches infinity.

3. Classification of interfaces: liquid/solid (L/S), gas/liquid (G/L), liquid/liquid (L/L) and gas/solid (G/S)

The emergence of interfaces for the synthesis of conducting polymers started from the idea of pickering emulsions. Pickering emulsions are composed of large particles, such as silicon

oxide, that stabilizes the emulsions by adsorbing to a liquid/liquid interface.[58] The liquid/liquid interface is the one that was extensively studied by researchers in the past decade.[20] Many variations of the liquid/liquid interfacial experimental setup have been tried by researchers to enable the effective nanostructure tuning of CPs. In 2013, the field of materials science witnessed the emergence of the gas/liquid interface by the synthesis of PPy/Ag films on the air/water interface.[61] The emergence of a solid ice surface as a novel template happened in 2015 with the work from the research group of Park *et al.*[62]

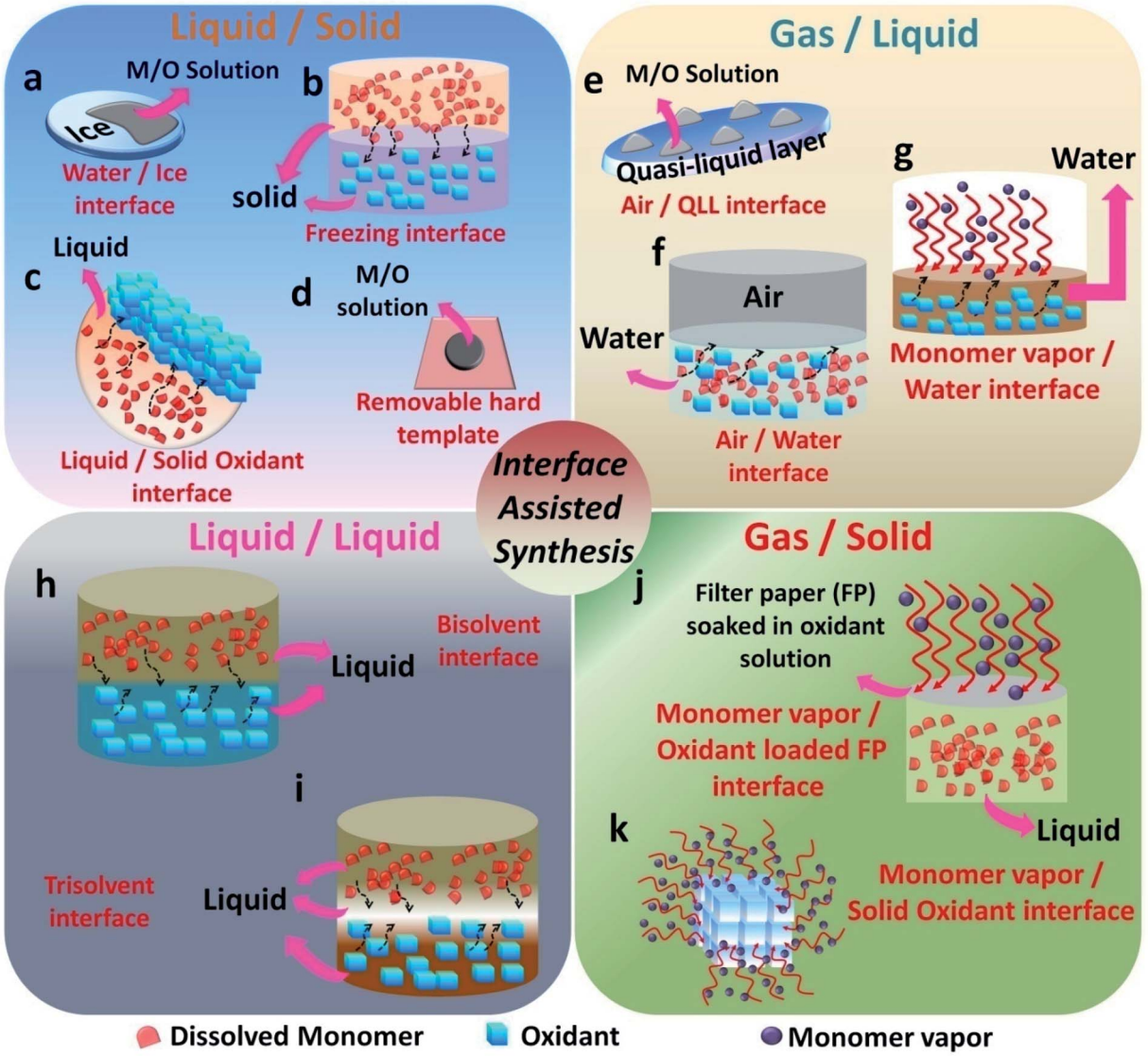

Fig. 2 Schematic illustration of CP synthesis assisted by four types of interfaces: liquid/solid interface (a–d), gas/liquid (e–g), liquid/liquid (h and i) and gas/solid (j and k). The black curved arrows indicate the directed motion of the respective reactants (monomer, oxidant or both). (a) Ice surface acting as a template for the synthesis of CPs. The aqueous solution of the monomer/oxidant mixture (M/O solution) was drop-casted on the ice surface, followed by deep freezing at −20 °C lead to the synthesis of CPs. (b) The freezing interfacial polymerization (FIP) at the freezing interface formed by two immiscible solvents at −20 °C acts to initiate the redox reaction. Monomer molecules are dissolved in the upper liquid phase and the oxidant molecules in the lower liquid phase. Both liquid phases become solidified at −20 °C. The reaction takes place at the interface between the liquid monomer and frozen lower solid phase. (c) Interface formed between a solid oxidant and an immiscible liquid. The monomer is dispersed in the liquid phase that acts as a nonsolvent for the oxidant crystals. (d) Polymerization on the surface of a removal hard template (*e.g.*, glass, filter paper). The M/O solution drop-casted on the surface of these templates initiates the polymerization in a liquid/solid interface of water and template. (e) Ice surface acting as a soft template. The sudden increase of the temperature from deep frozen state (−20 °C) to 0 °C leads to the melting of the ice surface and the formation of a quasi-liquid layer (QLL). The polymerization proceeds at the interface of air and QLL after the drop-casting of the M/O solution. (f) Both monomer and oxidant dissolved in the aqueous phase, and the polymerization starts at the air/water interface. Prior to the redox reaction, reactants diffuse to the interface, as shown in the form of a curved arrow. (g) The polymerization reaction at the interface of the monomer vapor phase and water. The oxidant molecules dissolved in the aqueous phase, and the monomer vapor molecules diffuse to the interface. The polymerization at the interface of (h) two liquids and (i) three liquids. (j) Vapor phase polymerization (VPP) at the interface of the monomer vapor and oxidant-loaded filter paper mounted on the surface of the aqueous monomer solution. (k) The polymerization at the interface of the monomer vapor and solid oxidant crystals.

This urged other researchers to find more and more solid templates (as a reaction field or precursor materials). The monomer vapors in the gaseous phase were employed as a template for the polymerization on the surface of solid oxidants.[63] This was a major breakthrough and after that, many variants of the gas/solid interfacial methods have been evolved. The interfaces that are involved in CP synthesis can be broadly classified in this review as liquid/solid (L/S), gas/liquid (G/L), liquid/liquid (L/L) and gas/solid (G/S) (Fig. 2). A liquid/solid (L/S) interface tunes the morphology in an effective way without the agglomeration or destruction of the polymer nanostructures.[56] In a typical L/S interfacial synthesis, the monomers are dissolved or dispersed in the solution phase. Conversely, the polymerization takes place at the interface, leading to hybrid materials. The solid phase takes the role of a template, reaction field or precursor by willingly providing its 2-D surface for the nanostructure control of CPs.[44] The successful alignment and orientation of the monomers in the 3-D space are achieved by the interaction forces with atoms or molecules of the solid surface.[44,62,64–66] After the removal of the solid template, the nature of the template will be reflected in the end macroscopic/microscopic morphology of the polymer and its hybrids. Many soft and hard templates have been reported as serving the role of solid templates for the nanostructure control of conducting polymers. Generally, hard templates direct the preferential 2-D orientation of monomers, and soft templates assists the oxidative polymerization of monomers in the solution phase.[62] Various polymer nanostructures ranging from nanoparticles,[67] nanotubes (NTs),[30] nanofibers (NFs),[68] nanowires (NWs), nanosheets (NSs)[69] and networks[42] have been synthesized by employing both soft and hard solid templates. Most of the previous studies have concentrated on graphene oxide (GO) as a hard template because of its 2-D nature in terms of the atomic level thickness and high surface area.[70–72] However, GO probably yields inhomogeneous structures, and very complex methods are required for the effective removal of GO from the composites.[62] This scenario demands the necessity for the introduction of new solid surfaces for the synthesis of CPs and its hybrids. Solid templates, such as ice, solvent crystals, precursor salts and glass, have emerged as promising materials for the morphology control of polymer nanostructures (Fig. 2a–d). The synthetic strategies based on the L/S interface provided by the aforementioned templates proved to be facile, low cost, and assured the easy removal of the templates too. In a typical gas/liquid (G/L) interfacial polymerization, the monomers are commonly present in the liquid phase, where they are dissolved in water (Fig. 2e–g). The air/water interface possesses a high value of surface tension, and inorganic/organic nanoparticles have a tendency to reduce this high tension through preferential adsorption on the interface.[58,59] The COP of CPs follows this mechanism in a typical air–water interface. The monomers and oxidants present in the aqueous phase tend to localize on the air/water interface for the polymerization reaction. The self assembly of the nanoparticles is driven by the combined effect of the 2-D nature of the G/L interface and the high surface tension of water.[20] In L/L interfacial polymerization, the initiators and monomers are dissolved in separate liquid phases (Fig. 2h and i). When the initiators and monomers diffuse to the L–L interface, polymerization is triggered. This interfacial system can produce homogeneous films or particles. As polymerization proceeds, the polymer gradually diffuses and fills either of the two phases or the interface, depending upon the polarity.[20] Therefore, the resulting amount of polymer material usually increases as the polymerization time increases. The high interfacial tension between the immiscible phases accounts for the dynamic self-organization of molecules at the interface.[20,29,59] During polymerization, the high interfacial tension drags the nanoparticle-attached oligomers or short chain polymers towards the interface. It promotes the secondary growth at the interface, leading to the 2-D morphology.[10] However, if the oligomer–solvent interaction exceeds the interfacial tension, the oligomers move towards the bulk solution, where it undergoes secondary growth. In addition, depending on the polarity of the selected solvents and the doped state of the polymer chains, the oligomers migrate to the successive phases. This leads to fibre or tube-like morphology.[18,73–75] Synthesis on solid surfaces under ultra-high vacuum or gas (G/S) is an efficient method for the synthesis of 2-D CP sheets and films with atomic thickness and periodic structure (Fig. 2j and k).[56,76] The high diffusion rate of the monomers under high vacuum and slow polymerization rate facilitates the formation of well-ordered structures. The past few decades have witnessed significant efforts in interface polymerization methods for the preparation of CPs. Considering the depth of the field, this review focuses only on polymerization methods controlled by different types of removable interfaces. This section discusses the recent trends in the field of interface-assisted polymerization methods for the synthesis of CPs and its hybrid systems. The synthesis methods are summarized under four categories: L/S, G/S, L/L and G/S.

3.1. L/S interface-assisted polymerization

In a typical L/S interfacial polymerization method, monomers are usually dispersed in a liquid phase, which is then allowed to react with the solid surface. The solid surface can be a 2-D template, which can simultaneously act as a template, precursor or reaction field. Based on the type of interaction that drives the delocalization of the monomer molecules, the L/S interfaces can be recognized into three types: ice surface, solvent crystals, precursor salts and other removal hard templates (cellulose paper, glass).

3.1.1. Ice surface: a potential 2-D template for self-assembled CP nanostructures. Ice-assisted chemistry is an emerging branch of low cost, environment-friendly and simple strategy for the synthesis of CP sheets and films.[62,64,65,77–80] The dimension-controlled synthesis of CPs and its hybrids is another noteworthy feature of the ice-templating synthesis. The ice surface provides a 2-D template, and the underlying mechanism of polymerization is the preferential self-organization of monomers through the weak hydrogen bonding interactions above.[62,64] Ice can be viewed as a removable hard template, in which the surface water molecules possessing lower potential energy than bulk water act as active sites for hydrogen bonding

interactions with the functional groups of the monomer molecules.[62,81] The very low reaction temperature (mostly ≤ -20 °C) and slow diffusion of the monomers from the liquid phase to the ice surface facilitates the controlled polymerization rates without any secondary growth of oligomer chains, giving highly crystalline 2-D polymer sheets/films.[56] The easy removal of ice by a simple melting process helps in obtaining high surface area pristine CP 2-D nanostructures.[62]

The use of the ice-templating method for the synthesis of CP sheets/films emerged with the synthesis of PANI nanosheets by Park *et al.* in 2015.[62] They successfully synthesized PANI nanosheets of a few millimeters in diameter on the ice surface

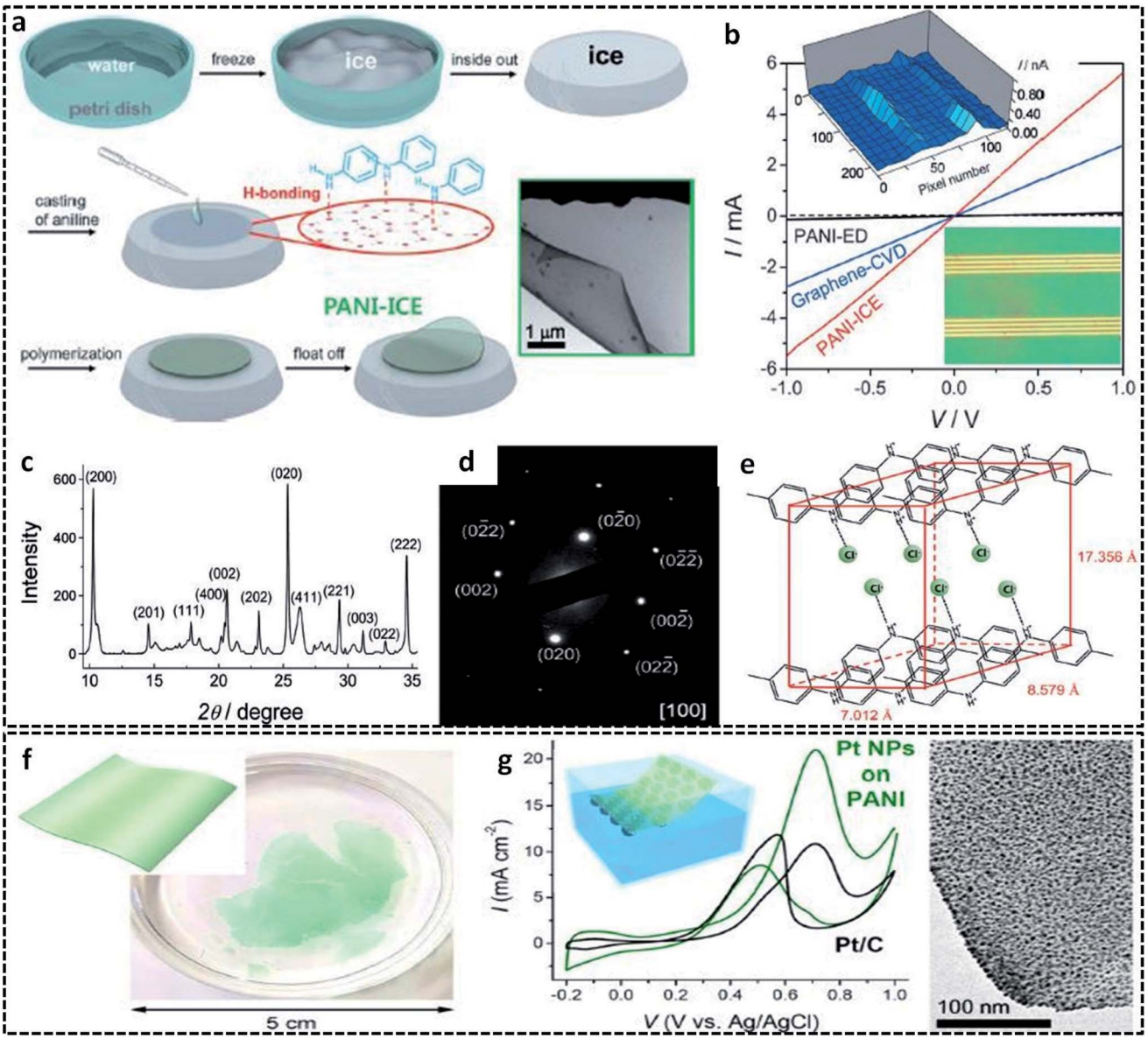

Fig. 3 (a) Schematic representation of the synthesis of the 2-D PANI sheets on the ice surface. The inset shows the HRTEM of the 2-D PANI sheets. (b) *I*–*V* characteristic curve of the PANI sheets in comparison with PANI-ED (PANI films synthesized by galvanostatic electrochemical deposition method) and graphene-CVD (graphene synthesized by conventional chemical vapor deposition method). Inset in the bottom right shows the optical image of the PANI 2-D sheets transferred to the gold electrodes. Inset in the top left shows the AFM height profile of the 2-D PANI sheets on the ice surface. The structural determination of the PANI 2-D sheets elucidated from (c) X-ray powder diffraction and (d) selected area electron diffractionindicate the highly crystalline PANI with an orthorhombic structure. (e) Illustration of the determined orthorhombic structure with edge-on π–π stacking. Reproduced with permission under a Creative Commons CC-BY License from ref. 62, Copyright 2015 John Wiley and Sons. (f) Photographic image of the PANI sheets prepared on the ice surface with inset showing a schematic representation of the PANI sheets. (g) CV profiles of the Pt NPs supported PANI nanosheets in comparison with the Pt NPs supported on carbon in an aqueous solution of 0.1 M $HClO_4$ and 1 M methanol at a scan rate of 50 mV s^{-1} and at a temperature of 25 °C. HRTEM image on the right corresponds to the uniform encapsulation of Pt NPs on the surface of the PANI sheets. The inset shows the schematic illustration of the PANI/Pt nanosheets suspended on the surface of water. Reprinted with permission from ref. 81. Copyright (2017) American Chemical Society.

through a COP of aniline (Fig. 3a). The ice surface provides a template for the preferential orientation of aniline monomers by the influence of surface water molecules having lower potential energy than the bulk molecules.[62,64] The homogenous adsorption of protonated anilinium ion on the dangling OH groups of the ice surface through hydrogen bonding and electrostatic interactions promotes the vertical growth of PANI on the ice surface. In detail, the synthesis method starts with the casting of an aniline solution in HCl on frozen ice in a Petri dish, followed by the addition of APS solution in HCl. A very low temperature of −20 °C not only inhibits the etching of ice, but also favors the slow and controlled polymerization of aniline. By a simple melting process, the template-free PANI nanosheets with a thickness of ∼30 nm can be retrieved from the Petri dish. After a reaction time of 3 min, the PANI nanosheets can be easily transferred to any substrates for further studies. The TEM image clearly shows the sheet morphology of PANI. The *I–V* characteristics in Fig. 3b clearly show a distinct high current of 5.5 mA at 1 V and a high electrical conductivity of 35 S cm^{-1} of the PANI nanosheets, which reveals a considerable improvement from the previously reported values of other PANI systems. The electronic structure and crystallinity of the obtained PANI sheets were confirmed by XRD and SAED (Fig. 3c and d). The aniline molecules in the PANI nanosheets are oriented through edge-on π–π stacking and have a long range order with an orthorhombic space group, with unit cell parameters of $a = 17.4$ Å, $b = 7.0$ Å, $c = 8.6$ Å, and $\alpha = \beta = \gamma = 90.00°$ (Fig. 3e). Contrary to other chemical oxidation polymerization techniques for synthesizing PANI nanostructures such as 0-D[67,82] or 1-D[83,84] morphologies, the facile route of the ice-assisted synthesis is really promising for the preparation of highly crystalline 2-D sheets. The same PANI 2-D nanosheets can be further utilized for the synthesis of hybrid structures. Park *et al.* used PANI nanosheets for the successful encapsulation of Pt nanoparticles by suspending the sheets on an air–water interface (Fig. 3f).[81] The PANI nanosheets suspended on the precursor solution of platinum nanoparticles act as a solid template (or L/S interface) for the clustering of Pt ions at the active molecular sites of PANI. The obtained PANI sheets were highly distributed with Pt nanoparticles (size of 2.7 nm) embedded on it. The PANI/Pt nanosheets showed high current densities and good performance towards methanol oxidation (Fig. 3g). The ice-assisted synthesis was also reported for the synthesis of PANI nanoparticles aided by surfactants, such as poly(2-acrylamido-2-methylpropanesulfonic acid) (PAAMPSA) and poly(4-styrenesulfonic acid) (PSSA).[64] The synthesis follows the same method discussed above, in which a stock solution of aniline/surfactant mixture in HCl was casted on deep frozen ice, followed by the addition of APS solution. The proposed mechanism of spherical PANI nanostructure formation is the surfactant assisted heterogeneous nucleation of aniline oligomers on the ice surface.[85]

The ice templating method can also be extended for other CP based systems for the synthesis of 2-D nanostructures. Self-standing PPy nanofilms were successfully synthesized on the ice–liquid interface offered by the frozen ice surface by COP of the pyrrole monomer.[77] In order to decrease the surface energy, the deep frozen ice is constructed with a little amount of ethanol. The smooth surface of the deep frozen ice at −20 °C is casted with ferric chloride ($FeCl_3$) solution in HCl, followed by pyrrole solution in ethanol (Fig. 4a). Considering the fact that the liquid phase (here ethanol) should have a very low melting point below −20 °C, this method also gives the freedom of choice of solvents based on this melting point constraint. The PPy nanofilms were formed at the ice/ethanol interface by varying the reaction time from 20 min to 6 h. The polymerization reaction was quenched by pouring water into the reaction vessel at room temperature, resulting in the formation of PPy films floating on water. In detail, the mechanism of the PPy film formation is driven by several molecular interactions, as we discussed earlier in the PANI nanosheets formation. The anchoring of the pyrrole molecules on the ice surface (ice/ethanol interface) by hydrogen bonding interactions facilitates the confined orientation of the pyrrole molecules, followed by the polymerization by Fe^{3+} ions. Initially, the PPy nanoparticles are formed at the ice/ethanol interface due to the lack of driving forces for the growth of PPy chains in two dimensions. However, the initially formed PPy nanoparticles are aggregated and self-assembled into PPy films by noncovalent interactions, such as π–π stacking, hydrogen bonding and van der Waals forces. As the reaction time increases, solid and free-standing low thickness PPy films are formed on the ice surface. Due to the lack of any organic sacrificial layer or toxic reagents, this low-cost method of synthesizing large area PPy films with controlled thickness is superior to many previous reports of nanofilm synthesis strategies.[86–88] The PPy nanofilm facing towards ice was found to be highly hydrophilic with a water contact angle (WCA) of 0° (Fig. 4b), and the side facing towards air showed a WCA of 82.3° (Fig. 4c). The thickness measurements from FESEM images are in agreement with those from the AFM scan technique (Fig. 4d and e). The selective adsorption of the pyrrole molecules on the ice/ethanol interface has been studied by molecular dynamics (MD) simulations. The theoretical model predicts that at the initial stage, the pyrrole molecules are randomly distributed in the ethanol phase (Fig. 4f). During the course of the reaction, the pyrrole molecules will get deposited on the ice surface through hydrogen bonding interactions between the amino group of pyrrole and hydroxyl group of water (Fig. 4g). The simulation results attributed to the above model show that about 60% of the total pyrrole molecules are deposited on the ice surface in a system of 10 : 70 ratio of pyrrole and ethanol molecules. The potential use of the ice template for the synthesis of PPy-based hybrid structures was also reported. The ice/ethanol interface was found to be an effective template for tailoring the morphology and electronic properties of the reduced graphene oxide (rGO)/PPy films (Fig. 4h).[89] The representative SEM images of the rGO/PPy films exhibit pristine film nature with no separate aggregation of the individual PPy nanoparticles (Fig. 4i). The uniform growth of PPy on the surface of the graphene oxide (GO) nanosheets is achieved by the trapping of the pyrrole molecules by oxygen-containing groups of GO. The rGO/PPy films were demonstrated as a flexible all-solid-state supercapacitor with high volumetric specific capacitance of 17.3 F cm^{-3}.

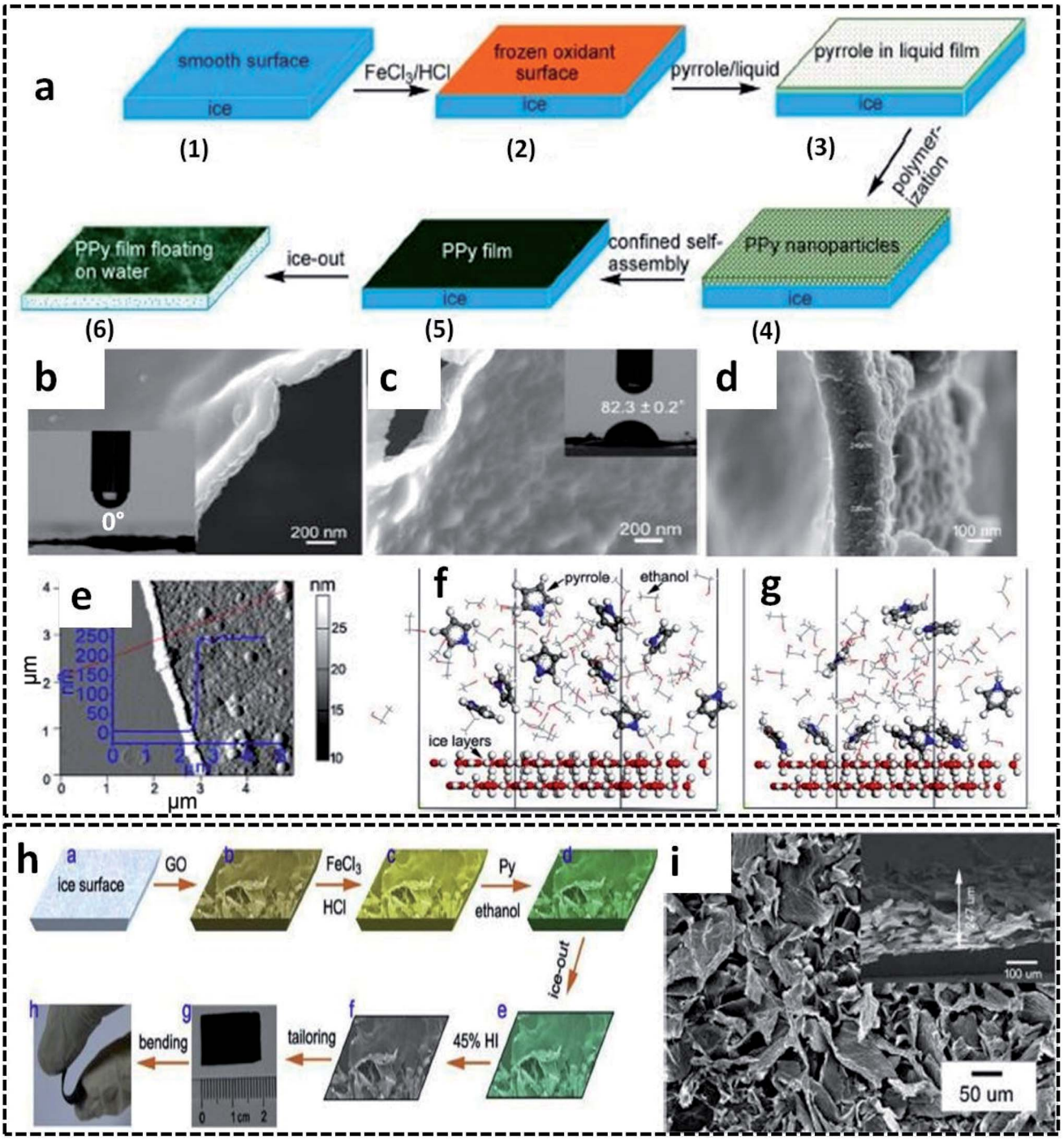

Fig. 4 (a) Schematic illustration of the synthesis of the PPy nanofilm in an ice/ethanol interface. SEM image of the PPy nanofilm: (b) with side towards the ice; (c) with side towards air; inset of (b) and (c) shows the photograph of WCA on the corresponding side (the corresponding WCA values written across the photograph); (d) cross-sectional image showing a thickness of 238 nm. (e) AFM image of the PPy nanofilm with inset showing the thickness profile along the red line. Molecular dynamics simulation corresponding to the adsorption of the pyrrole molecules on the ice surface: (f) initial stage; (g) equilibrium state. Adapted from ref. 77, Copyright (2017), with permission from Elsevier. (h) Schematic representation of the synthesis of rGO/PPy films on ice surface. (i) SEM image of rGO/PPy film with inset showing the SEM image of end face. Reprinted from ref. 89, Copyright (2018), with permission from Elsevier.

Another facile route of the liquid/solid interface-assisted synthesis of CP films was reported by Wang *et al.*[78] They named the method as the freezing interfacial polymerization (FIP) method. The FIP method shares the same mechanism as that of the ice-templating method discussed in previous sections. Here, a system of two immiscible solvents (cyclohexane and water) in a deep frozen state provides the liquid/solid interface for the chemical oxidation polymerization of

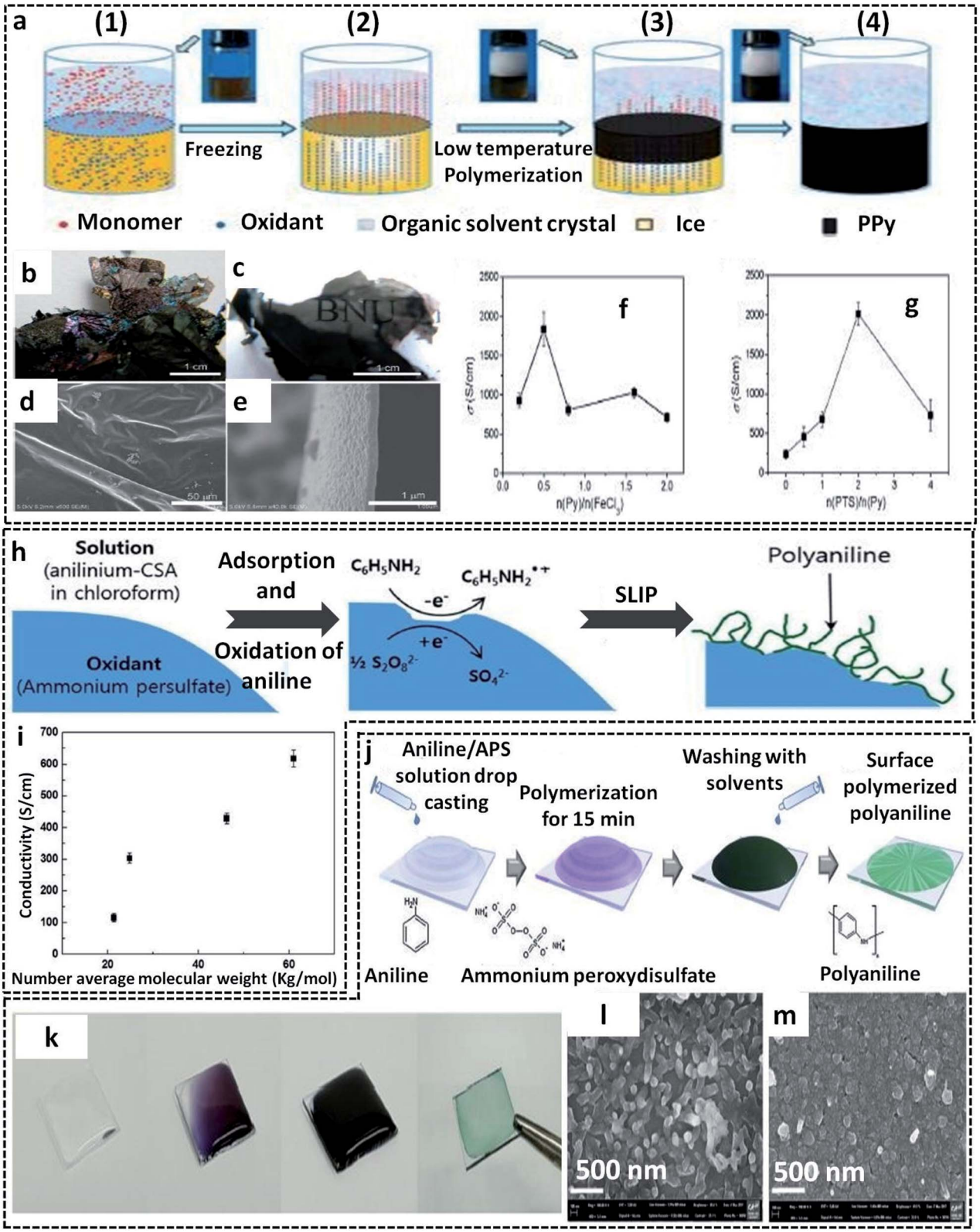

Fig. 5 (a) Schematic representation of the freezing interfacial polymerization method (FIP) for the preparation of PPy films. 1 to 4 represent various steps of FIP. In step 1, a clear formation of the interface takes place between the two immiscible liquids (cyclohexane and water). The system was subjected to undergo deep freezing at −20 °C in step 2, followed by the formation of solvent crystals. The pyrrole starts to expel from the upper organic phase to the lower aqueous phase. At the same time, the oxidant and dopant also get expelled from ice, where it reacts with the pyrrole monomer at the solid/liquid interface (steps 2 and 3). The formation of the PPy films is shown in step 4. (b and c) Photographic images of the PPy films showing the metallic luster and semi-transparency. SEM images of the PPy films from (d) top view and (e) cross-sectional view. The electrical conductivity plots of PPy films with different molar ratios of (f) pyrrole to $FeCl_3$ and (g) PTS to pyrrole. Adapted from ref. 78 with

pyrrole, resulting in large area PPy films (Fig. 5a). The system of cyclohexane/water was deep frozen at preferably (−10 to −20 °C), in which both solvents gradually crystallize. The pyrrole monomer dissolved in the upper organic phase (melting point, −23 °C) remains in the liquid state. As the reaction proceeds, the monomer molecules start migrating from the upper cyclohexane crystals to the lower aqueous phase through interstices. Meanwhile, the oxidant and dopant are expelled from the ice crystals to leave a dense layer. Due to the gravitational pull, the pyrrole molecules penetrate the ice interstices, where they meet the oxidant and dopant molecules. The COP of the pyrrole monomers is initiated and leads to the formation of insoluble free-standing highly crystalline PPy films. High quality large area CP films with excellent properties can be prepared using this method with careful optimization of the following: (1) monomer/oxidant/dopant amounts, (2) choice of solvent, and (3) reaction temperature. The photographic images of the as-prepared PPy films by FIP show a metallic luster and semi-transparency (Fig. 5b and c). The SEM images clearly show the smooth surface of the PPy films with a thickness of 100 nm (Fig. 5d and e). To fabricate PPy films with metallic luster and high electrical conductivity, $FeCl_3$ was chosen as the oxidant and *p*-toluenesulfonic acid (PTS) as the dopant. The PPy films showed a very high electrical conductivity of 2010 S cm^{-1}, in which the initial reactant molar ratio was pyrrole/$n(FeCl_3)$/n(PTS) = 1/2/2 (Fig. 5f and g).

3.1.2. Other solid surfaces as removal hard template. Other solid surfaces have been reported as soluble templates for the polymerization reactions. These materials not only act as reaction fields, but also take part in the polymerization reactions as precursor salts. For example, poly(methyl methacrylate) PMMA was synthesized on the surface of ferric chloride by a typical COP of methyl methacrylate (MMA) monomers.[90] The reaction vessel comprises a neat monomer liquid, along with solid precursor salts/oxidants.[91–93] PANI nanofibers were formed at the L/S interface offered by APS crystals.[66] Aniline and camphor sulfonic acid are dissolved in chloroform solvent, followed by the addition of finely powdered APS powder as the oxidant (Fig. 5h). The COP resulted in the formation of PANI nanofibers with high crystallinity, high molecular weight and high electrical conductivity (Fig. 5i), as compared with those produced by conventional solution polymerization methods.[29,42,48,85] PANI nanofibers of controllable sizes were also synthesized by using glass as a removable template.[94] The aqueous solutions of aniline and APS were casted one after another on the glass surface (water/glass interface), in which the polymerization was performed at room temperature for controlled time periods (Fig. 5j and k). The morphology was found to be nanofibrillar at low oxidant concentrations (Fig. 5l), and showed fused nanoparticle-like structures at high oxidant levels (Fig. 5m).

PPy nanosheets were synthesized on air-laid cellulose paper substrate suspended on an ice surface.[95] The overall synthesis procedure for preparing multilayer PPy nanosheets on the air-laid paper substrate is shown in Fig. 6a. Briefly, the airlaid paper soaked in APS solution was placed on ice at 0 °C. This was followed by the addition of the pyrrole monomer, leading to the controlled COP at 0 °C. The strong adhesion between the PPy nanosheets and paper substrate could be attributed to the hydrogen bonding interactions between the C–N bonds of pyrrole and the O–H bonds of cellulose. The presence of wrinkles in the multilayer PPy nanosheets (Fig. 6b) on the paper substrate opens the door for solar-thermal conversion through the efficient trapping of light. The transmittance spectra in Fig. 6c confirm that the multilayer PPy nanosheets can exhibit a distinct broadband absorption over a wide range of the solar irradiance spectrum. A solar-thermal conversion efficiency of 95.33% by multilayer PPy nanosheets on a paper substrate was reported to be superior to those of previously reported ones (Fig. 6d).

3.2. G/L interface-assisted polymerization

A G/L interface system comprises a monomer/oxidant solution, which was then allowed to polymerize in a 2-D confined space offered by air or vacuum in close proximity with the solution phase. 2-D PEDOT:PSS sheets are synthesized on the ice-surface through the COP of EDOT monomers at the air/water interface.[96] In brief, the reaction involves the casting of EDOT in acetone and the oxidant/dopant mixture (PSS/$FeCl_3$/$Na_2S_2O_8$/HCl) in water in deep frozen ice at −20 °C (Fig. 7a). A sudden increase of the reaction temperature from −20 °C to 0 °C leads to the melting of the ice at the air/water interface. This resulted in the formation of highly crystalline 2-D PEDOT/PSS sheets on the QLL above the ice surface. The obtained 2-D sheets have an electrical conductivity of 28 S cm^{-1} (Fig. 7b). The TEM and photographic images show the excellent large area sheet morphology of PEDOT/PSS with good transparency (Fig. 7c and d). Fig. 7e shows the 2-D crystal formation of the PEDOT/PSS sheets to be indexed to a monoclinic *P*2 space group. The TEM image in Fig. 7f confirms the highly crystalline phases, indicating the strong π–π stacked PEDOT molecules with a d-spacing of 3.4 Å. The XRD patterns further reveal the monoclinic phase of the PEDOT/PSS 2-D films and improved crystallinity compared with the bulk PEDOT/PSS nanostructures (Fig. 7g). The excellent properties of these 2-D sheets can be used for the fabrication of the photovoltaic devices with good current density and conversion efficiency. The surfactant-mediated air/water interface was employed for the synthesis of quasi 2-D (q2D) PANI films with good chemical vapor sensing ability.[97] The detailed synthesis strategy involves the localization of the surfactant molecules on air/water interface, followed

permission from the Royal Society of Chemistry. (h) Schematic representation of the synthesis of PANI nanofibers by S/L interfacial polymerization (SLIP) at the APS surface. (i) Variation of the electrical conductivity with the average molecular weight of PANI fabricated by the S/L interfacial method. Adapted from ref. 66 with permission from the Royal Society of Chemistry. (j) Schematic illustration of the PANI film synthesis at the surface of the glass substrate. (k) Photographic images of the PANI films on glass substrate. SEM images of the PANI films on the glass surface at (l) low oxidant amount and (m) high oxidant amount. Reprinted from ref. 94, Copyright (2018), with permission from Elsevier.

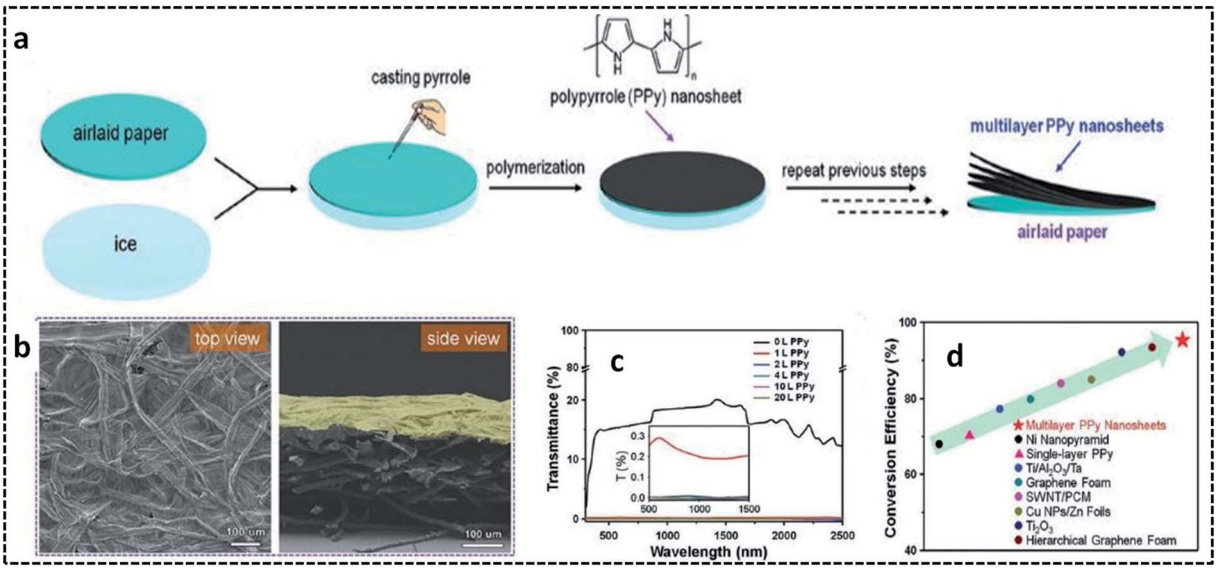

Fig. 6 (a) Schematic illustration of the overall fabrication process of the multilayer PPy nanosheets on a paper substrate. (b) SEM images of the airlaid paper coated with one layer of PPy nanosheet. (c) Transmittance spectra of the airlaid paper substrate coated with several layers of PPy nanosheets. (d) Solar-thermal conversion efficiency compared to previously reported materials. Reproduced with permission under a Creative Commons CC-BY License from ref. 95. Copyright 2019 John Wiley and Sons.

by the trapping of the protonated aniline oligomers by the anionic groups of the surfactant through hydrogen bonding interactions (Fig. 8a). The self-assembly of the aniline oligomers through π–π stacking results in elongated 2-D films at the air–water interface. The height profile shown in the AFM image (Fig. 8b) confirms the thickness of the q2D PANI films in a few nanometers. The single crystalline nature of the PANI films indexed to the monoclinic phase is also shown in the SAED pattern (Fig. 8c). The appealing high electrical conductivity of 160 S cm^{-1}, sensing towards ammonia and volatile organic compounds (VOCs) make the q2D PANI films as an emerging material in the field of thin film organic electronics (Fig. 8d). The air/water interface has been employed for the synthesis of PPy films using $FeCl_3$ as an oxidant by a simple step of rapid mixing COP (Fig. 8e).[98] The obtained films are composed of spherical PPy particles, as observed in Fig. 8f. Fig. 8g shows the dye-absorption properties of the PPy films in the presence of the anionic dye Eosin Yellow (EY). The photopolymerization of the pyrrole monomer in the presence of $AgNO_3$ at the air/water interface resulted in PPy/Ag films having an electrical conductivity of 14.9 S cm^{-1} (Fig. 8h and i).[61] The obtained PPy/Ag films are utilized as a substrate-free material for supercapacitors.[61]

A new method utilizing the intriguing properties of the gas/liquid interface was invented by D. Arcy *et al.*[99] They synthesized polypyrrole nanonets possessing high active surface area by a novel method of vapor–liquid interfacial polymerization. The distinct feature of this method is that the pyrrole monomer vapors itself act as a reactive field and precursor for the synthesis of the ultraporous PPy nanonets. Influenced by Langmuir–Blodgett surface dynamics, the synthesis mechanism conveys the role of the vapor/liquid interface for the polymerization of the pyrrole monomer vapor into the net morphology. These nanonets exhibit a remarkable specific capacitance of 518 F g^{-1} due to its high surface-to-volume ratio and porous structure. These exceptional properties of the PPy nanonets make them suitable materials for electrochemical capacitors. The synthesis procedure follows the COP of the pyrrole monomer vapor filled in a chamber containing a Petri dish with iron(III) tosylate aqueous solution as the oxidant (Fig. 9a). After 90 minutes of polymerization, an insoluble PPy film is formed at the vapor/liquid interface and can be easily separated (Fig. 9b). The nano-sized net morphology of the PPy films is evident in the SEM image (Fig. 9c). The AFM image in Fig. 9d reveals the distinct 150 nm thick polypyrrole nanonets.

3.3. L/L interface-assisted polymerization

The L/L interface polymerization can be considered to be the first interfacial technique emerging as an effective synthesis method of CP-based systems. The monomers/oxidants are dissolved in respective immiscible solvents, leading to the formation of a visible 2-D interface. The L/L interface provides the freedom of choice of solvents and oxidants since the interfacial tension values control the fate of polymerization.[20] Our research group has synthesized PPy/Ag hybrid sheets by a facile route of water–chloroform interface-assisted polymerization method.[10] The pyrrole oligomers dispersed in chloroform solvent are subjected to undergo migration towards the interface where they meet the oxidant, $AgNO_3$. The COP between the monomer and the oxidant resulted in the formation of PPy/Ag hybrid sheets. The type of oxidant and the interfacial tension was observed to control the end polymer morphology. The redox reaction between the oxidant ($AgNO_3$) and pyrrole monomer results in the formation of Ag NPs attached to the oligomer chains (Fig. 9e). The high interfacial tension of the water/chloroform system drags the NP-attached pyrrole oligomers

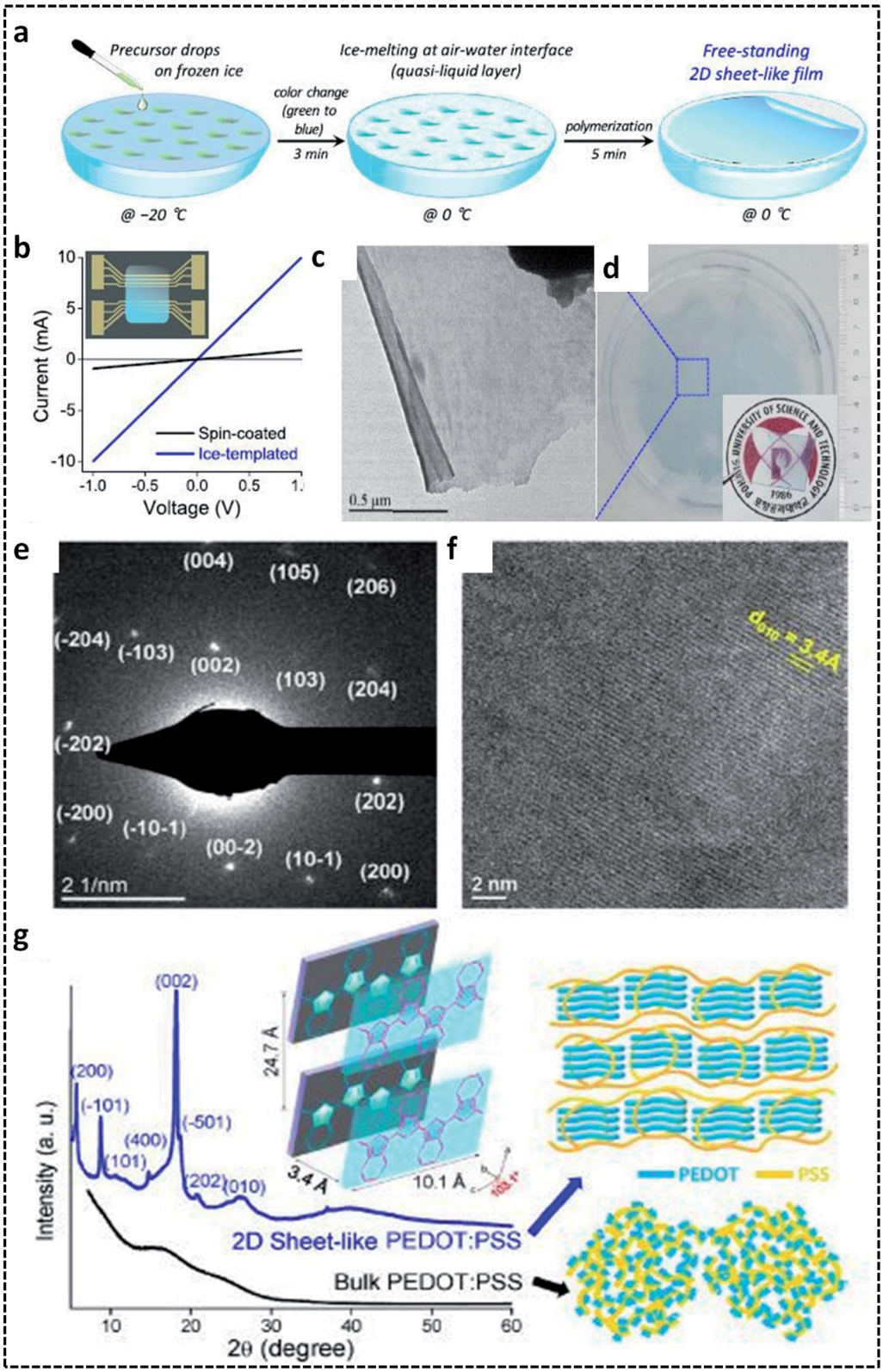

Fig. 7 (a) Schematic illustration of the formation of 2-D PEDOT/PSS sheets on the air/water interface. (b) *I*–*V* plot of the 2-D PEDOT/PSS sheets. (c) TEM image of the 2-D PEDOT/PSS. (d) Photographic image of the semi-transparent 2-D PEDOT/PSS sheet-like film. (e) SAED pattern of the 2-D PEDOT/PSS sheets indexed to the monoclinic *P*2 space group. (f) HRTEM image showing the highly crystalline nature of the 2-D PEDOT/PSS sheets. (g) XRD spectra of the 2-D PEDOT/PSS sheets with schematic representation of the π–π stacking between the PEDOT chains. Reprinted with permission from ref. 96. Copyright (2019) American Chemical Society.

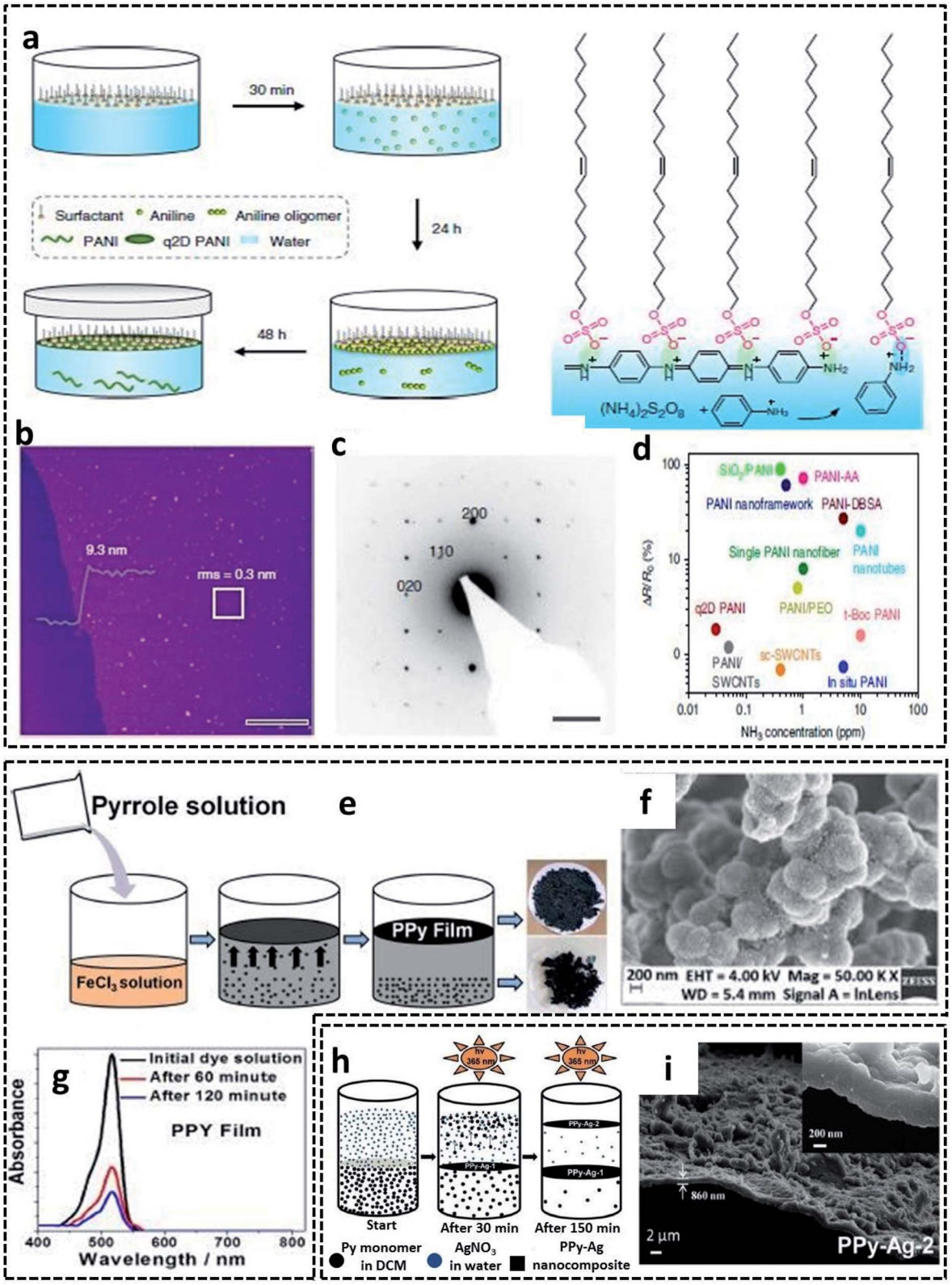

Fig. 8 (a) Schematic representation of the surfactant-assisted synthesis of the q2D PANI films on the air/water interface. (b) AFM image of the q2D PANI films with the height profile. (c) SAED pattern showing the single crystalline nature of the q2D PANI films. (d) Ammonia sensing performance of the q2D PANI films compared with other PANI-based sensors. (e) Schematic representation of the PPy films synthesized on the air/water interface. (f) SEM image showing the spherical PPy particles on the film surface. (g) Time-dependent UV-visible absorbance plot of the EY dye-adsorption. Reproduced with permission under a Creative Commons CC-BY License from ref. 98. (h) Schematic illustration of PPy/Ag hybrid films synthesized by photopolymerization on air/water interface. (i) SEM of PPy/Ag hybrid films synthesized by photopolymerization on air/water interface. Adapted from ref. 61 with permission from the Royal Society of Chemistry.

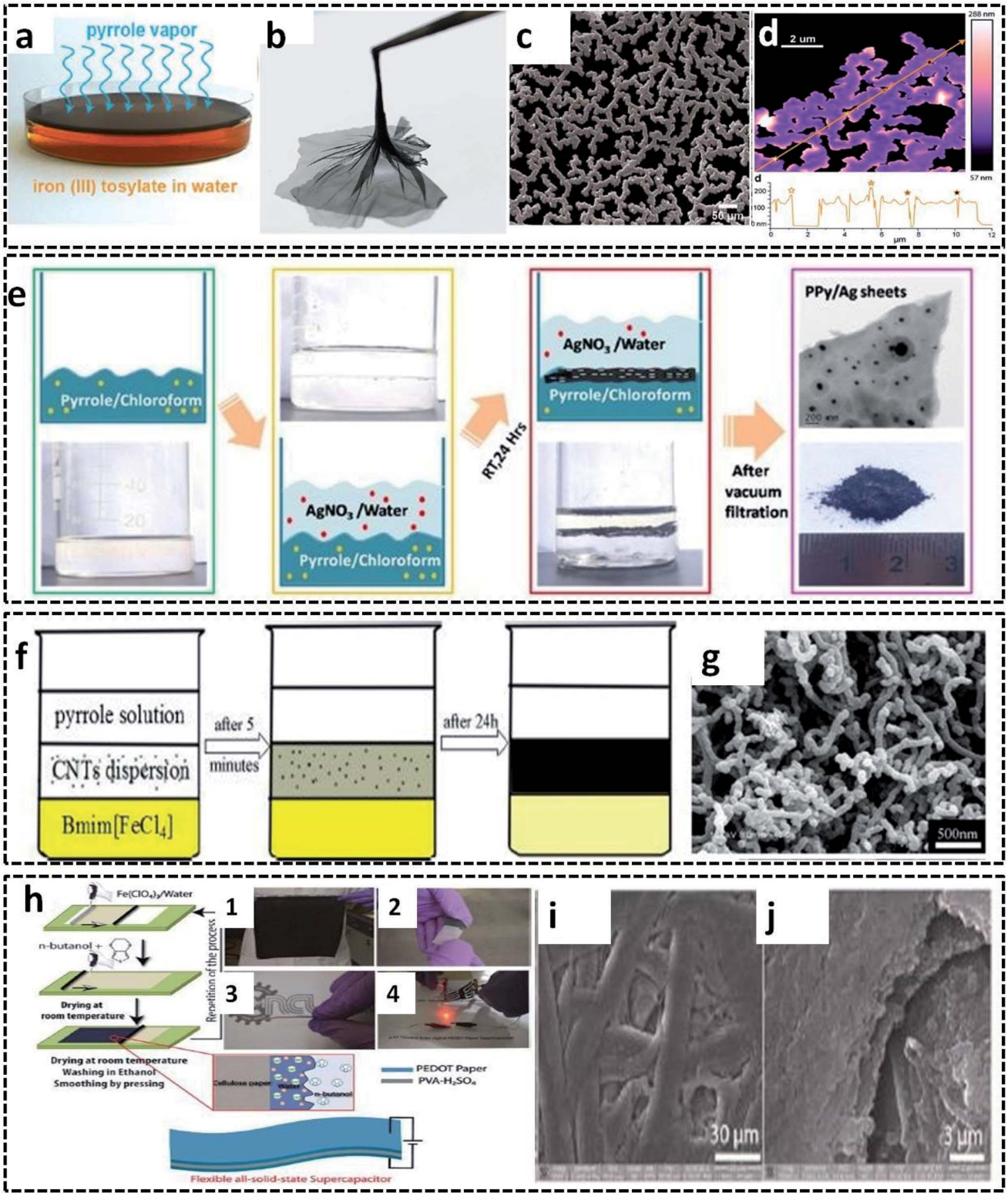

Fig. 9 (a) PPy nanonet synthesis setup. (b) Photographic image of the PPy nanonet film. SEM (c) and AFM (d) images of the purified PPy nanonet. Reproduced from ref. 99 with the permission of the Royal Society of Chemistry. Schematic representation of the (e) water–chloroform-assisted synthesis of PPy/Ag sheets, along with the TEM image of the PPy/Ag sheet. Reprinted with permission from ref. 10. Copyright (2019) American Chemical Society. (f) Ternary phase interfacial synthesis of PPy/MWCNT. (g) SEM image of PPy/MWCNT. Reprinted from ref. 100, Copyright (2012), with permission from Elsevier. (h) Schematic illustration of the synthesis of the PEDOT/cellulose paper by L/L interfacial polymerization for the fabrication of all solid-state flexible supercapacitor. (h-1) Photographic image of the PEDOT/cellulose paper. (h-2) Photographic image of the surface of clean scotch tape peeled off from the PEDOT/cellulose paper. (h-3) Photographic image of a flexible all-solid-state supercapacitor made from PEDOT/cellulose paper. (h-4) Photographic image of an interdigital supercapacitor made from a flexible single layer PEDOT/cellulose paper, which glows under LED. (i and j) SEM images of the PEDOT/cellulose paper. Reproduced from ref. 101 with the permission of the Royal Society of Chemistry.

towards it, and leads to the formation of PPy/Ag hybrid sheets. However, the pristine PPy was formed with spherical morphology in the same bisolvent system due to the lack of metal NPs. Thus, the study of CP morphology tuning by L/L interface opens new possibilities for the preparation of hybrid materials for multifunctional applications. The PPy/Ag hybrid sheets showed good redox properties that urged us to analyze the electrochemical detection of hydrogen peroxide. Due to the uniform distribution of Ag NPs in the PPy sheets, as can be seen from the TEM image in Fig. 9e, it was also used as antibacterial agents against Gram-positive and Gram-negative bacteria. Zhang *et al.* used a ternary system of solvents for the interfacial polymerization of pyrrole for the synthesis of the PPy/MWCNT hybrids (Fig. 9f).[100] The synthesis procedure involves the system of three immiscible liquid phases: (1) the oxidant solution containing 1-butyl-3-methylimidazoliumtetrachloroferrate (Bmim[$FeCl_4$]) in hexane at the bottom, (2) MWCNT dispersion on top of it, and (3) pyrrole monomer solution in water. As the reaction proceeds, a black product of PPy/MWCNT is formed. The SEM image clearly shows the complete encapsulation of CNT by polypyrrole (Fig. 9g). Kurungot *et al.* synthesized the highly conducting PEDOT on a flexible cellulose paper by interfacial polymerization method.[101] The EDOT monomer dissolved in *n*-butanol was subjected to react with iron perchlorate ($Fe(ClO_4)_3$) in water, leading to the formation of PEDOT uniformly distributed on cellulose paper (Fig. 9h). The SEM images confirm the uniform attachment of PEDOT on cellulose paper (Fig. 9i and j). The PEDOT/cellulose paper was found to exhibit a high electrical conductivity of 375 S cm^{-1}, along with high specific capacitance of 115 F g^{-1} and high volumetric capacitance of 145 F cm^{-3}.

Polythiophene/gold (PTh/Au) hybrid films were prepared by a water/hexane interface-assisted polymerization method.[102] The aqueous solution of tetrachloroauric acid acts as the source of gold NPs and the oxidant for the COP of thiophene dissolved in *n*-hexane. The PTh/Au films are uniformly distributed with Au NPs of 2.1 nm (Fig. 10a). The provisions for the easy transfer of PTh/Au films to any substrate make it an efficient material for applications, such as solar cells, electrochromic devices and flexible electronic devices. An ionic liquid/water interfacial system was found to be effective for the synthesis of Janus-type polythiophene/gold composites.[21] The Janus-type PTh/Au composite shows microurchin shapes on the side facing water and dendritic nanofiber morphology on the side facing ionic liquid (Fig. 10b and c). This variable trend in morphology in the same bisolvent system reveals that the limited diffusion of monomers and oxidant at the L/L interface also controls the polymer morphology. The L/L interface-assisted COP is also widely reported for the synthesis of polypyrrole/metal NPs hybrid systems in huge numbers. A facile one-pot interfacial synthesis in a bisolvent system of water and chloroform was employed for the preparation of PPy/platinum (PPy/Pt) composites.[103] The PPy/Pt composites were mainly of granular morphology with a uniform distribution of Pt NPs with an average size distribution of 2.5 nm. The composites were selected for the fabrication of modified electrodes for the electrochemical sensing of hydrogen peroxide. The L/L interfacial polymerization of pyrrole can also be finely tuned by the aid of some specific surfactants. A binary surfactant system of Span 80/OP 10 was identified to carry out the effective morphology tuning of polypyrrole in a bisolvent interface of water and chloroform.[104] As the HLB (hydrophile–lipophile balance) value of the surfactant increases, the morphology of the polypyrrole ranged from a ruptured vesicle-like structure to a coral-like structure (Fig. 10d-1 and d-2). The 1-D CP nanostructures were synthesized by L/L interfacial synthesis method. Highly conducting nanocables of PEDOT/Au were synthesized by the water/dichloromethane bisolvent system. The nanocables have a very high electrical conductivity of 770 S cm^{-1} (Fig. 10e).[2] A PbTe-based hybrid system with PEDOT nanotubes was reported to have good thermoelectric properties (Fig. 10f).[105] The 1-D nanotubes of PEDOT were synthesized by microemulsion interfacial polymerization method. The obtained PEDOT nanotubes were used for the fabrication of chemical sensors towards alcohol vapors (Fig. 10g).[106]

3.4. G/S interface-assisted polymerization

The vapor phase polymerization (VPP) can be performed not only in the G/L liquid system, but also at the G/S interface. Here, the monomer vapors are forced to undergo COP at the G/S interface offered by the oxidant solid crystals. The oxidant crystals act as both reaction template and precursor material for the synthesis of CP and its hybrid nanostructures. VPP is also a 2-D confined reaction, in which the nanostructure of the CPs can be controlled at a slow polymerization rate. Nanosheets of PPy, PEDOT and PANI were successfully prepared by VPP at the surface of $CuCl_2 \cdot H_2O$, which acts as an oxidant and template (Fig. 11a).[63] Argon was used as the carrier gas to carry the monomer vapor to the surface of the finely powdered oxidant crystals. The mechanism of polymerization at the gas/solid interface is very intriguing for the material scientists. The inert gas carrying the monomer vapor was forced to diffuse to the surface oxidant crystals. The adsorbed species react with the oxidant at the growth site, and leads to the formation of polymer nanosheets. The adsorbed nanosheets are desorbed for the further reaction pathway. The gas/solid interface plays a crucial role in tuning the 2-D sheet morphology by controlling the slow polymerization rate. The nanosheet morphology of the CP nanosheets is evident from the representative SEM and AFM images (Fig. 11b–g). A similar synthesis strategy has been employed for the preparation of PPy on cellulose filter paper (PPy–FP) (Fig. 11h).[107] The FP dipped in the initiator solution was suspended on the pyrrole monomer solution to achieve the polymerization of pyrrole vapors on the surface of FP. The reaction resulted in the formation of uniformly distributed PPy on the surface of FP (Fig. 11i). The FP modified with highly conducting PPy was used for the sensing of ammonia vapor (Fig. 11j).

4. The role of interfaces in tuning the nanostructure of CP based systems

The various types of interfaces, generalized mechanism of polymerization at interfaces, and diverse synthesis

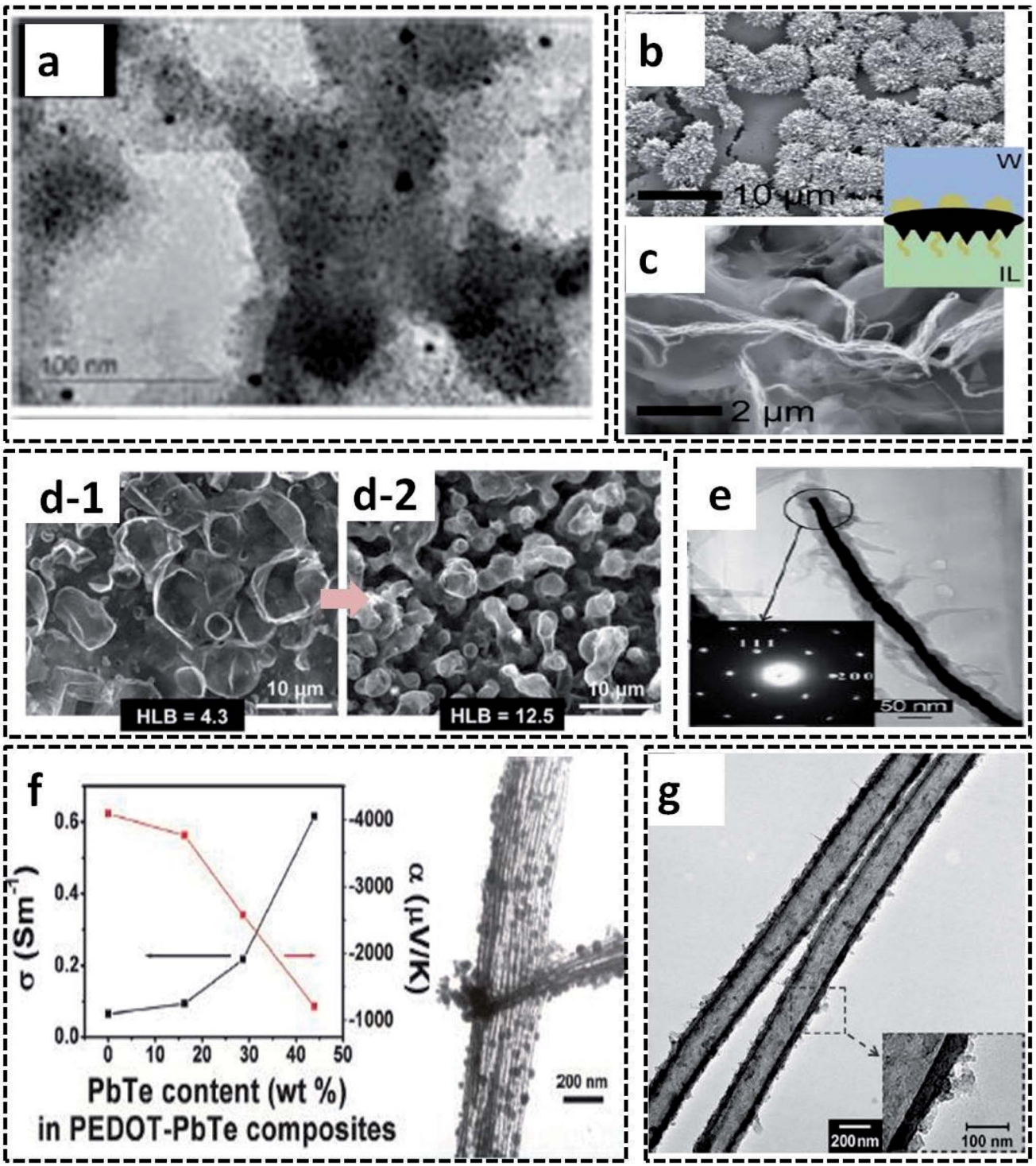

Fig. 10 (a) TEM images of the PTh/Au film. Reprinted from ref. 102, Copyright (2018), with permission from Elsevier. SEM images of (b) microurchin and (c) dendrite-like fiber shapes of the PTh/Au composite prepared by ionic liquid/water interfacial polymerization. Reprinted with permission from ref. 21. Copyright (2018) American Chemical Society. (d) SEM images of PPy synthesized by water/chloroform interface-assisted polymerization in the presence of a surfactant mixture (Span 80 and OP 10). The transformation of the morphology from a ruptured vesicle type to coral type is shown in the figure with an arrow. Reprinted from ref. 104, Copyright (2018), with permission from Elsevier. (e) TEM image of PEDOT/Au nanocable with inset showing the SAED pattern of the highly crystalline Au. Reprinted with permission from ref. 2. Copyright (2007) American Chemical Society. (f) TEM image of the PEDOT–PbTe composite tubes showing thermoelectric property. Reprinted with permission from ref. 105. Copyright (2011) American Chemical Society. (g) The TEM image of the 1-D PEDOT nanotubes prepared by water in oil micro-emulsion interfacial polymerization method. Reproduced with permission under a Creative Commons CC-BY License from ref. 106. Copyright 2007 John Wiley and Sons.

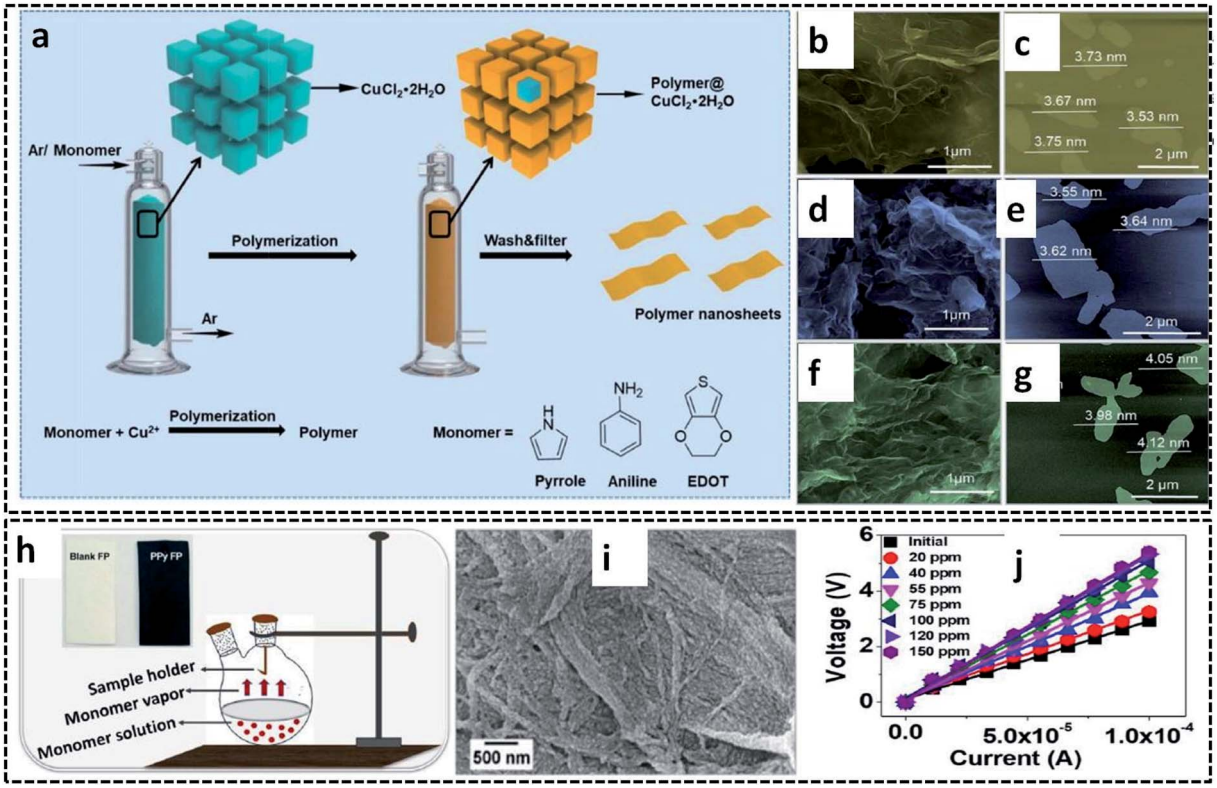

Fig. 11 (a) Schematic diagram of VPP for the synthesis of PPy, PEDOT, and PANI nanosheets on the gas/solid interface. (b) SEM image and (c) AFM image of the PPy nanosheets. (d) SEM image and (e) AFM image of the PANI nanosheets. (f) SEM image and (g) AFM image of the PEDOT nanosheets. Reproduced from ref. 63 with the permission of the Royal Society of Chemistry. (h) Schematic diagram of VPP of PPy–FP. (i) SEM image of PPy–FP. (j) *I*–*V* plot of PPy–FP at different concentrations of ammonia vapor. Reprinted with permission from ref. 107. Copyright (2020) American Chemical Society.

methodologies to control the nanostructure of CPs have been discussed in the previous sections. As already discussed, any interface can be viewed as an imaginary 2-D surface that is capable of modulating the self-assembly process at the interface, and subsequently control the CP nanostructure.[20,56,57,60b,108] Considering the inherent 2-D nature of the interface, the CP based systems tend to orient in a 2-D manner along the interface.[56,57] However, different interfaces may tune the CP nanostructure in diverse manners depending on the various interaction forces developed at the interface, which directs the

Table 1 The various types of interfaces, interactive forces at interfaces, and their role in controlling the nanostructure of various CP-based systems

Sl. no.	Type of interface	Role of interface	Resultant nanostructures	CP-based systems
1	Ice/water, ice/ethanol, freezing interface, air/QLL, cellulose filter paper/pyrrole	Surface for the controlled orientation of monomer or oligomers by intermolecular hydrogen bonding	2-D (nanosheets, nanofilms, large scale films)	PANI[62] PPy[77,78,95] PPy/rGO[89] PEDOT:PSS[96]
2	APS crystal/chloroform, monomer vapor/$CuCl_2 \cdot H_2O$	Nanostructure controlling template as observed in oxidant crystals	1-D nanofibers, 2-D nanosheets	PPy[63] PEDOT[63] PANI[63,66]
3	Glass/water	Insoluble hard template	1-D nanofibers	PANI[94]
4	Air/water, binary and tertiary L/L, monomer vapor/water	Surface for the preferential adsorption of nanoparticles by virtue of interfacial tension	0-D granules, 1-D (rod, nanotubes, nanocables), 2-D (films, sheets), 3-D porous networks	PPy[98–100,104] PPy/Ag[10,61] PANI[97] PPy/Pt[103] PTh/Au[21,102] PEDOT/Au[2] PEDOT/PbTe[105] PEDOT[106]

preferential orientation of reactive molecules. Based on the interaction forces between the interface and the reactive molecules, the interface may act as a: (1) surface for the controlled orientation of monomer or oligomers by intermolecular hydrogen bonding,[62,65,77,78,89,95,96] (2) nanostructure-controlling template as observed in oxidant crystals,[44,63,66] (3) insoluble hard templates,[44,94] and (4) surface for the preferential adsorption of nanoparticles by virtue of the interfacial tension.[2,10,20,21,59,61,97–100,102–106] The various types of interfaces, interactive forces at interfaces, and their role in controlling the nanostructure of various CP-based systems is tabulated in Table 1.

Interfaces formed by templates, such as ice,[44,62,77,78,89] quasi-liquid layer[65,96] and cellulose filter paper[95] at stringent low temperature conditions ($\leq$0 °C) control the orientation of monomers or oligomers (Table 1, sl. no. 1). These templates can act as nanoreactors for the selective adsorption of monomers through intermolecular hydrogen bonding between the active functional groups of the monomer or oligomer and the O–H groups of water or cellulose.[44,62,65,77,78,95,96] The intermolecular hydrogen bonding is responsible for the oriented edge-on π–π stacking of monomers or oligomers, leading to highly crystalline 2-D CP sheets or films.[62,77,78,89,95,96] The ice-templated synthesis methods involving interfaces such as ice/water, ice/ethanol and cellulose filter paper/pyrrole assures an easy retrieval or separation of products from the reaction medium.[62,77,95] Additionally, this synthesis is devoid of any highly toxic chemicals as solvents.[77] The stringent low temperature conditions established by ice template synthesis limit the possibilities of temperature optimizations during polymerization. The freezing interface follows the mechanistic pathway, in which the interstices of the solid crystals act as the template for the S/L interfacial polymerization.[78] The slow and controlled polymerization rate offered by the freezing interface, as well as the controlled orientation of monomers mediated by ice crystals, leads to high quality large area 2-D films.[78] However, the use of toxic organic solvents for the synthesis may lower the potential of the FIP method.[77,78] As shown in Table 1, sl. no. 2, the crystal surface of the oxidants can serve the role of a precursor, as well as template, for the successful nanostructure tuning of CPs.[44,63,66] The APS crystal/chloroform interface was observed to tune the 1-D nanofiber morphology of the PANI nanostructures.[66] On the contrary, the controlled adsorption and desorption of the monomer vapors on $CuCl_2 \cdot H_2O$ resulted in 2-D nanosheets of PPy, PANI and PEDOT.[63] The subsequent purification steps enable the successful separation of products from the unreacted crystal surfaces. The inherent 1-D nanofibrillar morphology of the PANI nanostructures was reflected in the glass/water interface during the COP of the aniline monomer with APS.[94] An insoluble hard template, such as glass (as shown in Table 1, sl. no 3), will act as an unreactive template for polymerization. Since glass is a hard template, it is difficult to retrieve large area films from the glass surface.[109] The tabulated set of interfaces, corresponding to Table 1, sl. no. 4, determines the nanostructure of the CP-based systems with the aid of interfacial surface tension. Here, the driving force for the self organization of reactive molecules is the high interfacial tension between the phases.[10,20] Thus, a careful choice of solvent system and/or use of structure guiding agents and oxidant type may control the morphology of the polymer, ranging from 0-D to 3-D.[2,10,21,61,97–100,102–106] The products formed in the interfaces tabulated in Table 1, sl. no. 4 can be retrieved or separately very easily. However, the binary or tertiary mixtures may use toxic organic solvents.

In general, the inherent 2-D nature of the interface may direct the polymer nanostructure in to 2-D sheets or films, unless a structure guiding agent is introduced.[56,57] Furthermore, interfaces that assist the orientation of reactive molecules through weak intermolecular forces furnish 2-D films or sheets with long range order and high crystallinity. However, most of the interface techniques promote the morphological tuning into 2-D nanostructures; hence, major optimizations are

Table 2 The nanostructures and electrical conductivity of CPs synthesized by different chemical methods comprising dilute polymerization, surfactant mediated dilute polymerization, hard template-assisted dilute polymerization, electrochemical polymerization and interfacial polymerization

Sl. no.	CP system	Method of preparation	Resultant morphology	Electrical conductivity (S cm^{-1})
1	PPy	Surfactant-mediated dilute polymerization	1-D nanotubes[30]	49.8
2	PPy	Dilute polymerization	1-D nanotubes[30]	1.55
3	PANI	Dilute polymerization	2-D flakes[110]	473
4	PEDOT:PSS	Dilute polymerization	Nanostructure not mentioned[111]	453
5	PPy	Electrochemical polymerization	2-D films[112]	4500
6	PPy	Hard template assisted dilute polymerization	1-D nanotubes[113]	2
7	PANI	Water/ice interface polymerization	2-D nanosheets[62]	35
8	PPy	FIP	2-D films[78]	2010
9	PEDOT:PSS	Air/QLL polymerization	2-D sheets[96]	28
10	PANI	APS crystal/chloroform interface polymerization	1-D nanofibers[66]	580 $\pm$ 40
11	PANI	Glass/water interface polymerization	1-D nanofibers[94]	22.2
12	PANI	Surfactant mediated air/water interface polymerization	2-D films[97]	160
13	PPy	Surfactant mediated L/L interface polymerization	3-D porous network[104]	0.056
14	PPy	L/L interface polymerization	2-D free standing films[109]	560
15	PPy	G/S VPP	2-D nanosheets[63]	9.6

required for the synthesis of nanostructures having different dimensions.

5. Performance evaluation of CP nanostructures

In order to substantiate the relative performance of various interface methods, the electrical conductivity of CP nanostructures synthesized by diverse interfaces were analyzed. Furthermore, the electrical conductivity was used for validating the performance of pristine CPs in comparison with other chemical methods. The CP nanostructures synthesized by interfaces that tune the polymer morphology through interaction forces showed conductivity values ranging from 9.6 to 2010 S cm^{-1} (Table 2, sl. no. 7 to 12, 14–15).[62,63,66,78,94,96,97,109] The edge-on π–π stacking of monomers or oligomers resulted in highly conducting 2-D PPy films, as observed in the FIP method.[44,78] The high conductivity of the 1-D fibrous PANI synthesized on the oxidant crystal surface possessed high electrical conductivity (580 S cm^{-1}) by virtue of the enhanced crystalline intermolecular packing of high molecular weight polymers.[66] The high interfacial tension of the water/cyclohexane interface accounts for the high conductivity (560 S cm^{-1}) of the PPy films.[109] The self-organization of monomers, mediated by the influence of the air/water interfacial tension and surfactant, resulted in conductive 2-D PANI films showing a value of 160 S cm^{-1}.[97] The PPy nanosheets polymerized at the G/S interface by exposing the oxidant in the monomer vapor exhibited a conductivity of 9.6 S cm^{-1}.[63] Interestingly, 3-D porous networks of PPy formed at the L/L interface in the presence of surfactants exhibited relatively lower conductivity of 0.056 S cm^{-1}.[104] Based on the above observations, the interfaces that act as surfaces for the controlled orientation of reactive molecules may result in polymers having an appreciable value of electrical conductivity.

The relevance of the interface-assisted methods in synthesizing the CPs in comparison with other chemical methods has been validated on the basis of the electrical conductivity, as shown in Table 2. The different methods, such as dilute polymerization, electrochemical polymerization, hard template-assisted polymerization and surfactant-assisted polymerization, were compared with the interfacial-assisted synthesis methods. As discussed previously, the interface-assisted polymerization provides a relatively good electrical conductivity (9.6–2010 S cm^{-1}).[62,63,66,78,94,96,97,109] The dilute polymerization and hard template-assisted dilute polymerization produced 1-D nanotubes with very low value of electrical conductivity.[30,113] This can be attributed to the absence of driving forces for tuning the controlled self-assembly process and CP nanostructures.[10,20] The surfactants are introduced to lift the electrical conductivity values of the 1-D nanotubes to higher orders. These surfactants can act as structure guiding agents for the controlled growth of polymers by restricting the secondary growth.[30] Interestingly, the PPy nanostructures synthesized using chemical methods, such as dilute polymerization, hard template-assisted polymerization and surfactant-assisted polymerization, exhibited conductivity values of up to ~50 S cm^{-1}.[30,113] However, the electrochemical polymerization of pyrrole leads to a conductivity of 4500 S cm^{-1}, which could be attributed to the presence of *p*-toluenesulfonate as a large doping anion attached to the polymer chains.[112] The major limitation of electrochemical methods is that the PPy films have to subsequently peel off from the electrode surface; hence, it will be difficult to obtain large area CP films for the electrodeposited products.[109] The dilute polymerization resulted in a comparable electrical conductivity of ~500 S cm^{-1} for PANI[110] and PEDOT:PSS.[111] The interface methods were found to be successful in synthesizing PPy nanostructures with a good electrical conductivity, as compared to other methods.[78] In comparison with other methods, the PANI nanofibers prepared by S/L interfacial polymerization showed comparable value of electrical conductivity.[66] However, PEDOT:PSS synthesized by dilute polymerization was found to be superior in terms of its high electrical conductivity, as compared to other chemical methods.[111]

6. Future perspectives: a major insight into some potential applications of the interfacially synthesized CP based systems

The detailed mechanism and various possibilities of each type of interface resulting from the binary combinations of three states of matter, in tuning the structural, chemical and physical properties of conducting polymers, were discussed in the previous sections. This section aims to provide insight into the extension of these interface-assisted strategies to emerging technologies. The roots of each interface-assisted method have opened a portal for synthesizing novel CP hybrid systems for a wide range of potential applications. Thus, as a future outlook, the interface-assisted methods proposed in this review open doors for the synthesis of interesting CP based hybrids for multifunctional applications. A large number of solid substrates have emerged as efficient templates for the growth of CP based hybrid assemblies. Cellulose nanofibril films (CNF) have been reported as excellent templates due to its greater flexibility, lightweight property, and unique structure. CNF films coated with polypyrrole exhibits a good electrical conductivity of 23.77 S cm^{-1}.[114] The high electrical conductivity, good flexibility, high mechanical strength and unchangeable sheet resistance values even on different bending cycles display the intriguing performance of PPy/CNF films. A composite structure of porous melamine foam/PPy (MF/PPy) has evolved as a potential flexible and compressible supercapacitor.[115] The redox polymerization of pyrrole takes place in the interface of water and cyclohexane in the presence of MF (Fig. 12a). The MF not only acts as a template, but also provides a highly porous and compressible skeleton for the overall structure. These attractive properties of MF/PPy are ideal for the fabrication of flexible and compressible energy storage devices. The digital photos in Fig. 12b exhibit the superior tensile strength of MF/PPy composites. Furthermore, the utilization of MF/PPy electrodes in energy storage devices is investigated, as shown in

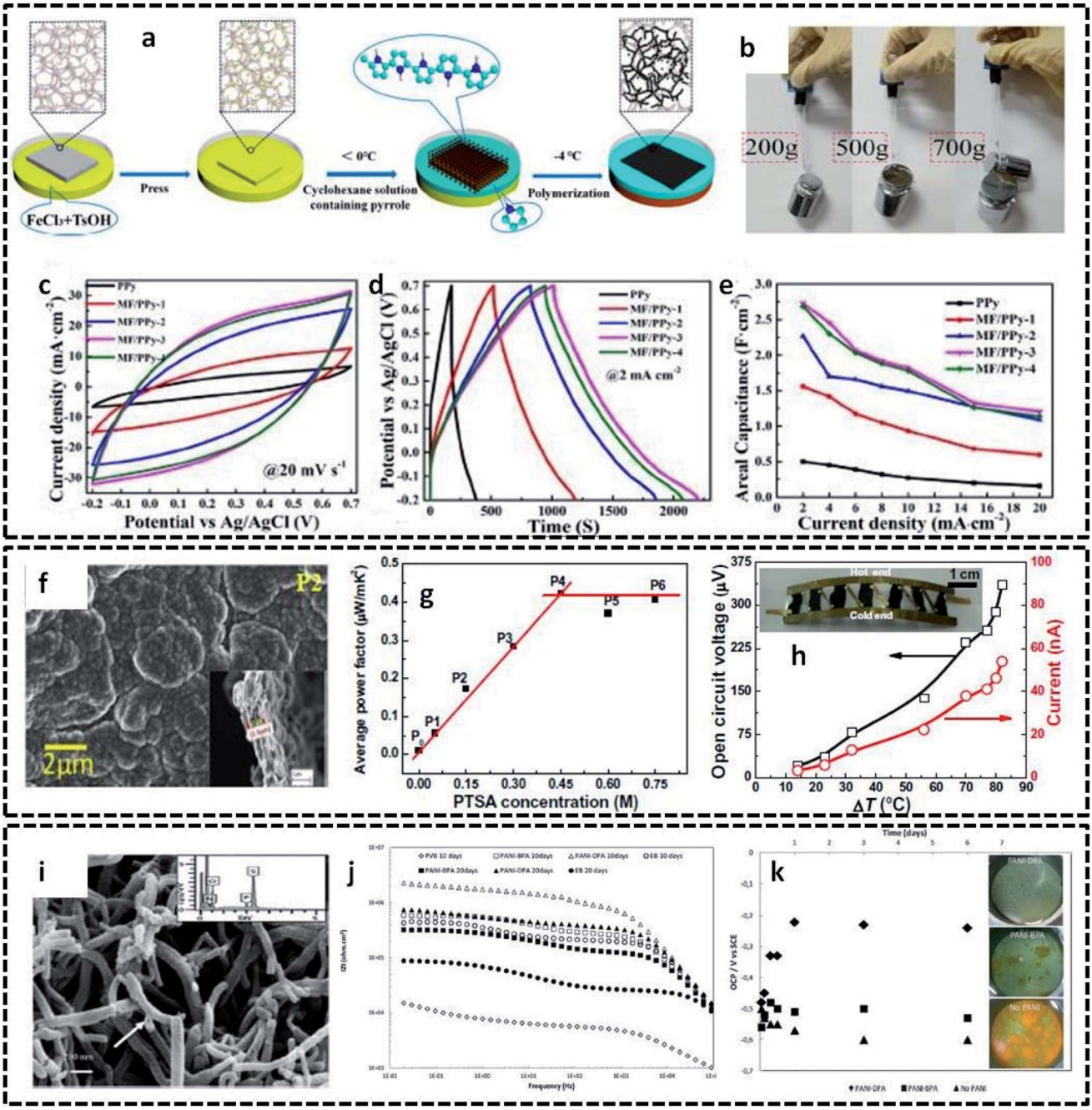

Fig. 12 (a) Schematic representation of the synthesis of flexible and compressible MF/PPy porous materials. Prior to the interfacial polymerization, the melamine foam (MF) was soaked in the initiator solution ($FeCl_3$ and TsOH). The reaction proceeds by the addition of cyclohexane containing the monomer. By cooling the bisolvent system to −4 °C, the polymerization takes place at the interface, whereas the MF acts as a template for the formation of porous MF/PPy composites. MF/PPy 1 to MF/PPy 4 represent the samples prepared at different polymerization times. (b) Photographic images displaying the tensile strength of MF/PPy. (c) CV curves of MF/PPy at 20 mV s^{-1}. (d) GCD curves at a current density of 2 mA cm^{-2}. (e) Rate capabilities showing the areal capacitance. Reprinted from ref. 115, Copyright (2019), with permission from Elsevier. (f) SEM image of free-standing PPy films prepared at the interface of cyclohexane and water. (g) Variation of average power factor with different concentrations of *para*-toluene sulphonic acid (PTSA) as the dopant. P1 to P6 correspond to different samples prepared at varying concentrations of PTSA. (h) Open circuit voltage and current generated for the flexible organic thermoelectric generator fabricated in the form of a wrist-band. Inset shows the photographic image of the wrist-band type device. Reprinted from ref. 116, Copyright (2019), with permission from Elsevier. (i) SEM image of PANI nanotubes prepared at the interface of aqueous/organic liquids. (j) Impedance spectra of steel specimens coated with PVB coatings only and PVB coatings with 0.5 wt% PANI synthesized in the presence of surfactants (BPA and DPA). (k) Variation of OCP with time for coatings with and without PANI in 3.5% NaCl solution. Inset shows the corrosive nature of the samples after 1 week immersion test. Reproduced from ref. 117 with permission from the PCCP Owner Societies.

Fig. 12c–e. The good reversibility and large enclosed area, as shown in the CV (Fig. 12c), indicate the good specific capacitance of MF/PPy. The GCD curves in Fig. 12d and e show a very high areal capacitance value (2.685 F cm^{-2}) for the fabricated electrodes. Bharti *et al.* successfully employed interfacially synthesized PPy films in the fabrication of wearable devices.[116] They utilized the cyclohexane/water interface for the preparation of free-standing PPy films. The outstanding properties of the PPy films made it possible to find applications in a wristband type thermoelectric power generator. The SEM image of the PPy film clearly shows a compact-type granular morphology (Fig. 12f). The PPy films show an average power factor of 0.45 μW mK^{-2} (Fig. 12g). The fabricated device possesses an open circuit voltage of 336 μV and current of 46 nA at 80 °C (Fig. 12h). PANI nanotubes were synthesized in an aqueous/organic interface in the presence of surfactants, such as benzylphosphonic acid (BPA) and decylphosphonic acid (DPA).[117] The pristine PANI nanotubes were employed in the synthesis of anticorrosive coatings. The SEM image (Fig. 12i) shows the tubular nature of PANI. The value of the low frequency impedance retains a high value for coatings with PANI nanotubes, as shown in the EIS spectra (Fig. 12j). The stable open circuit voltage of the coatings with PANI shows the appreciable anticorrosive property of the PANI nanotubes (Fig. 12k).

Less studies have been conducted on the synthesis of CPs in a system of monomer/oxidant in solid states (S/S interface).[92,93] The lack of mechanistic support diminishes the possibilities of this interface in synthesis. The detailed computational and mechanistic studies could be extended to interfaces other than L/S and L/L. This will give more insight into the kinetic and thermodynamic control of interface polymerization. The investigation of novel materials for use as templates in the synthesis of conducting polymers is at its infancy. Hence, the synthesis of CP based hybrids by the utilization of novel materials as templates would be a promising work in the near future.

7. Conclusions

In conclusion, this review tried to summarize the recent trends in the interface-assisted polymerization methods, and proved to be an efficient method for the successful nanostructure tuning of conducting polymers. To the best of our knowledge, there are no reports that conclusively discuss the interfacial polymerization methods for the synthesis of conducting polymers and its hybrid systems. The capability of the interfacial polymerization methods in diverse nanostructure tuning is hitherto undreamt of. The chemistry, mechanism and various types of interfaces have been discussed in detail. The detailed reports of each interface method intensify the possibilities and challenges in introducing the CP based systems for multifunctional applications. The interfaces discussed in this review are removable templates due to the lower complexity in separating the products from the respective interfaces. Different interfaces tune the polymer morphology in different ways, even if all interfaces share the same chemistry. The interaction forces between the interface and reactive molecules have an important role in the nanostructure of the CP based systems. Since almost all interfaces act as a 2-D template for the nanostructure tuning, the 2-D CP sheets and films have been reported in huge numbers until now. The dependence of various chemical methods of polymerization on the electrical conductivity of pristine CP nanostructures was also analyzed. The exceptional properties of the 2-D structures, like high surface to volume ratio, high porosity, single layer or multilayer thickness, makes them suitable candidates for applications, such as supercapacitors, sensors, flexible electronics and corrosion protection.[56,57]

Author contributions

The manuscript was written through the contributions of all authors. All authors have given approval to the final version of the manuscript.

Funding sources

M. M. M. greatly acknowledges the funding from the Science and Engineering Research Board (EEQ/2019/000606), and DST-INSPIRE (DST/INSPIRE/04/2015/002050) by the Department of Science and Technology (DST), India.

Conflicts of interest

The authors declare no conflict of interest.

References

1 L. Yuan, C. Wan, X. Ye and F. Wu, *Electrochim. Acta*, 2016, **213**, 115–123.
2 G. Lu, C. Li, J. Shen, Z. Chen and G. Shi, *J. Phys. Chem. C*, 2007, **111**, 5926–5931.
3 B. Anothumakkool, R. Soni, S. N. Bhange and S. Kurungot, *Energy Environ. Sci.*, 2015, **8**, 1339–1347.
4 Y. Chen, K. Cai, C. Liu, H. Song and X. Yang, *Adv. Energy Mater.*, 2017, **7**, 1701247.
5 F. Gao, N. Zhang, X. Fang and M. Ma, *ACS Appl. Mater. Interfaces*, 2017, **9**, 5692–5698.
6 X. Lu, W. Zhang, C. Wang, T. Wen and Y. Wei, *Prog. Polym. Sci.*, 2011, **36**, 671–712.
7 D. Wei, X. Lin, L. Li, S. Shang, M. C. Yuen, G. Yan and X. Yu, *Soft Matter*, 2013, **9**, 2832–2836.
8 B. H. D. Tran, D. Li and R. B. Kaner, *Adv. Mater.*, 2009, **21**, 1487–1499.
9 E. Mazzotta, A. Caroli, E. Primiceri, A. G. Monteduro, G. Maruccio and C. Malitesta, *J. Solid State Electrochem.*, 2017, **21**, 3495–3504.
10 S. K. Chondath, R. R. Poolakkandy, R. Kottayintavida, A. Thekkangil, N. K. Gopalan, S. T. Vasu, S. Athiyanathil and M. M. Menamparambath, *ACS Appl. Mater. Interfaces*, 2019, **11**, 1723–1731.
11 A. J. Marsden, D. G. Papageorgiou, C. Vallés, A. Liscio, V. Palermo, M. A. Bissett, R. J. Young and I. A. Kinloch, *2D Mater.*, 2018, **5**, 032003.

12 C. Li, H. Bai and G. Shi, *Chem. Soc. Rev.*, 2009, **38**, 2397–2409.
13 J. Stejskal, I. Sapurina and M. Trchová, *Prog. Polym. Sci.*, 2010, **35**, 1420–1481.
14 A. J. Heeger, *J. Phys. Chem. B*, 2001, **105**, 8475–8491.
15 M. Wan, *Macromol. Rapid Commun.*, 2009, **30**, 963–975.
16 A. G. MacDiarmid and A. J. Epstein, *Makromol. Chem., Macromol. Symp.*, 1991, **51**, 11–28.
17 J. Hazarika and A. Kumar, *J. Phys. Chem. B*, 2017, **121**, 6926–6933.
18 J. Li, Q. Jia, J. Zhu and M. Zheng, *Polym. Int.*, 2008, **57**, 337–341.
19 N. Nuraje, K. Su, N. Yang and H. Matsui, *ACS Nano*, 2008, **2**, 502–506.
20 P. Dallas and V. Georgakilas, *Adv. Colloid Interface Sci.*, 2015, **224**, 46–61.
21 N. Nishi, I. Yajima, K. Amano and T. Sakka, *Langmuir*, 2018, **34**, 2441–2447.
22 X. Yang and Y. Lu, *Mater. Lett.*, 2005, **59**, 2484–2487.
23 M. B. González, L. I. Brugnoni, M. E. Vela and S. B. Saidman, *Electrochim. Acta*, 2013, **102**, 66–71.
24 O. N. Efimov and T. Vernitskaya, *Russ. Chem. Rev.*, 1997, **66**, 443–457.
25 A. I. Hofmann, W. T. T. Smaal, M. Mumtaz, D. Katsigiannopoulos, C. Brochon, F. Schütze, O. R. Hild, E. Cloutet and G. Hadziioannou, *Angew. Chem., Int. Ed.*, 2015, **54**, 8626–8630.
26 D. Ni, Y. Chen, H. Song, C. Liu, X. Yang and K. Cai, *J. Mater. Chem. A*, 2019, **7**, 1323–1333.
27 G. Wang, A. Morrin, M. Li, N. Liu and X. Luo, *J. Mater. Chem. B*, 2018, **6**, 4173–4190.
28 J. Huang and R. B. Kaner, *Angew. Chem., Int. Ed.*, 2004, **43**, 5817–5821.
29 H. D. Tran, Y. Wang, J. M. D. Arcy and R. B. Kaner, *ACS Nano*, 2008, **2**, 1841–1848.
30 J. Stejskal, M. Trchová, P. Bober, Z. Morávková, D. Kopecký, M. Vrňata, J. Prokeš, M. Varga and E. Watzlová, *RSC Adv.*, 2016, **6**, 88382–88391.
31 E. Alekseeva, P. Bober, M. Trchová, I. Šeděnková, J. Prokeš and J. Stejskal, *Synth. Met.*, 2015, **209**, 105–111.
32 F. Liu, Y. Yuan, L. Li, S. Shang, X. Yu, Q. Zhang, S. Jiang and Y. Wu, *Composites, Part B*, 2014, **69**, 232–236.
33 S. Wang and G. Shi, *Mater. Chem. Phys.*, 2007, **102**, 255–259.
34 J. Wu, X. Zhang, T. Yao, J. Li, H. Zhang and B. Yang, *Langmuir*, 2010, **26**, 8751–8755.
35 S. Xing and G. Zhao, *Mater. Lett.*, 2007, **61**, 2040–2044.
36 M. F. Attia, T. Azib, Z. Salmi, A. Singh, P. Decorse, N. Battaglini, H. Lecoq, M. Omastová, A. A. Higazy, A. M. Elshafei, M. M. Hashem and M. M. Chehimi, *J. Colloid Interface Sci.*, 2013, **393**, 130–137.
37 Y. Wei, L. Li, X. Yang, G. Pan, G. Yan and X. Yu, *Nanoscale Res. Lett.*, 2010, **5**, 433–437.
38 J. Kawakita, J. M. Boter, N. Shova, H. Fujihira and T. Chikyow, *Electrochim. Acta*, 2015, **183**, 15–19.
39 K. Jlassi, A. Singh, D. K. Aswal, R. Losno, M. Benna-Zayani and M. M. Chehimi, *Colloids Surf., A*, 2013, **439**, 193–199.
40 A. R. Zanganeh and M. K. Amini, *Electrochim. Acta*, 2007, **52**, 3822–3830.
41 M. G. Han and S. H. Foulger, *Chem. Commun.*, 2005, 3092–3094.
42 Y. Zhu, H. He, M. Wan and L. Jiang, *Macromol. Rapid Commun.*, 2008, **29**, 1705–1710.
43 J. Huang and R. B. Kaner, *Chem. Commun.*, 2006, 367–376.
44 Y. Oaki, *J. Mater. Chem. A*, 2018, **6**, 23197–23219.
45 H. K. Chitte, G. N. Shinde, N. V. Bhat and V. E. Walunj, *J. Sens. Technol.*, 2011, **01**, 47–56.
46 M. F. Ghadim, A. Imani and G. Farzi, *J. Nanostruct. Chem.*, 2014, **4**, 1–5.
47 Y. Zhu, D. Hu, M. Wan, L. Jiang and Y. Wei, *Adv. Mater.*, 2007, **19**, 2092–2096.
48 Y. Zhu, J. Li, M. Wan and L. Jiang, *Macromol. Rapid Commun.*, 2008, **29**, 239–243.
49 J. Lee, H. Jeong, R. Lassarote Lavall, A. Busnaina, Y. Kim, Y. J. Jung and H. Lee, *ACS Appl. Mater. Interfaces*, 2017, **9**, 33203–33211.
50 D. Y. Chung, M. J. Kim, N. Kang, J. M. Yoo, H. Shin, O. H. Kim and Y. E. Sung, *Chem. Mater.*, 2017, **29**, 2890–2898.
51 R. R. Poolakkandy, S. K. Chondath, N. Puthiyottil, D. Davis and M. M. Menamparambath, *Langmuir*, 2020, **36**, 872–879.
52 H. Lee, H. Kim, M. S. Cho, J. Choi and Y. Lee, *Electrochim. Acta*, 2011, **56**, 7460–7466.
53 K. K. Kim, A. Hsu, X. Jia, S. M. Kim, Y. Shi, M. Hofmann, D. Nezich, J. F. Rodriguez-nieva, M. Dresselhaus, T. Palacios and J. Kong, *Nano Lett.*, 2012, **12**, 161–166.
54 L. Torini, J. F. Argillier and N. Zydowicz, *Macromolecules*, 2005, **38**, 3225–3236.
55 E. L. Wittbecker and P. W. Morgan, *J. Polym. Sci., Part A: Polym. Chem.*, 1996, **34**, 521–529.
56 R. Dong, T. Zhang and X. Feng, *Chem. Rev.*, 2018, **118**, 6189–6325.
57 L. Wang, H. Sahabudeen, T. Zhang and R. Dong, *npj 2D Mater. Appl.*, 2018, 1–7.
58 J. Frelichowska, M. Bolzinger and Y. Chevalier, *J. Colloid Interface Sci.*, 2010, **351**, 348–356.
59 V. A. Turek, M. P. Cecchini, J. Paget, A. R. Kucernak, A. A. Kornyshev and J. B. Edel, *ACS Nano*, 2012, **6**, 7789–7799.
60 (*a*) J. Ji, J. M. Dickson, R. F. Childs and B. E. Mccarry, *Macromolecules*, 2000, **33**, 624–633; (*b*) Y. Song, J. Fan, S. Wang and J. Fan, *Mater. Chem. Front.*, 2017, **1**, 1028–1040.
61 A. Singh, Z. Salmi, P. Jha, N. Joshi, A. Kumar, P. Decorse, H. Lecoq, S. Lau-Truong, D. K. Aswal, S. K. Guptaa and M. M. Chehimi, *RSC Adv.*, 2013, **3**, 13329–13336.
62 I. Y. Choi, J. Lee, H. Ahn, J. Lee, H. C. Choi and M. J. Park, *Angew. Chem., Int. Ed.*, 2015, **54**, 10497–10501.
63 L. Huang, Z. Guo, K. Liu, L. Xiong, L. Huang, X. Gao, J. Wu, J. Wan, Z. Hu and J. Zhou, *J. Mater. Chem. A*, 2019, **7**, 24929–24936.
64 S. K. Jang, J. Choi and F. S. Kim, *J. Nanosci. Nanotechnol.*, 2017, **17**, 7793–7798.
65 K. Kim and M. J. Park, *Nanoscale*, 2020, **12**, 14320–14338.
66 C. Kim, W. Oh and J. Park, *RSC Adv.*, 2016, 82721–82725.

67 H. Gao, T. Jiang, B. Han, Y. Wang, J. Du, Z. Liu and J. Zhang, *Polymer*, 2004, **45**, 3017–3019.
68 D. Jin, Z. Qin, Y. Shen, T. Li, L. Ding, Y. Chen and Y. Zhang, *J. Solid State Electrochem.*, 2018, **22**, 1227–1236.
69 H. Ghadimi, M. R. Mahmoudian and W. J. Basirun, *RSC Adv.*, 2015, **5**, 39366–39374.
70 M. Mitra, S. T. Ahamed, A. Ghosh, A. Mondal, K. Kargupta, S. Ganguly and D. Banerjee, *ACS Omega*, 2019, **4**, 1623–1635.
71 H. Wang, Q. Hao, X. Yang, L. Lu and X. Wang, *ACS Appl. Mater. Interfaces*, 2010, **2**, 821–828.
72 C. Paper, S. Anodic, D. Wang, F. Li, J. Zhao, W. Ren, Z. Chen, J. Tan, Z. Wu, I. Gentle, G. Q. Lu and H. Cheng, *ACS Nano*, 2009, **3**, 1745–1752.
73 H. Mao, X. Liu, D. Chao, L. Cui, Y. Li, W. Zhang and C. Wang, *J. Mater. Chem.*, 2010, **20**, 10277–10284.
74 S. Xing, G. Zhao and Y. Yuan, *Polym. Compos.*, 2008, **29**, 22–26.
75 J. Upadhyay, A. Kumar, B. Gogoi and A. K. Buragohain, *Mater. Sci. Eng., C*, 2015, **54**, 8–13.
76 L. Lafferentz, V. Eberhardt, C. Dri, C. Africh, G. Comelli, F. Esch, S. Hecht and L. Grill, *Nat. Chem.*, 2012, **4**, 215–220.
77 N. Bai, Z. Xu, Y. Tian, L. Gai, H. Jiang, K. Marcus and K. Liang, *Electrochim. Acta*, 2017, **249**, 360–368.
78 G. Qi, L. Huang and H. Wang, *Chem. Commun.*, 2012, **48**, 8246–8248.
79 G. Kim, C. Jo, W. Kim, J. Chun, S. Yoon, J. Lee and W. Choi, *Energy Environ. Sci.*, 2013, **6**, 2932–2938.
80 D. Barpuzary, K. Kim and M. J. Park, *ACS Nano*, 2019, **13**, 3953–3963.
81 K. Kim, H. Ahn and M. J. Park, *ACS Appl. Mater. Interfaces*, 2017, **9**, 30278–30282.
82 G. M. Neelgund and A. Oki, *Polym. Int.*, 2011, **60**, 1291–1295.
83 Y. Long, Z. Chen, N. Wang, Y. Ma, Z. Zhang, L. Zhang and M. Wan, *Appl. Phys. Lett.*, 2003, **83**, 1863–1865.
84 H. D. Tran, J. M. D. Arcy, Y. Wang, P. J. Beltramo, A. Strong and R. B. Kaner, *J. Mater. Chem.*, 2011, **21**, 3534–3550.
85 L. I. Dan, J. Huang and R. B. Kaner, *Acc. Chem. Res.*, 2009, **42**, 135–145.
86 J. Jang and J. H. Oh, *Adv. Funct. Mater.*, 2005, **15**, 494–502.
87 B. Li, Y. Xu, J. Chen, G. Chen, C. Zhao, X. Qian and M. Wang, *Appl. Surf. Sci.*, 2009, **256**, 235–238.
88 M. Nakata, M. Taga and H. Kise, *Polym. J.*, 1992, **24**, 437–441.
89 X. Guo, N. Bai, Y. Tian and L. Gai, *J. Power Sources*, 2018, **408**, 51–57.
90 Z. Yang, H. Peng, W. Wang and T. Liu, *J. Appl. Polym. Sci.*, 2010, **116**, 2658–2667.
91 S. Palaniappan and P. Manisankar, *Mater. Chem. Phys.*, 2010, **122**, 15–17.
92 C. F. Zhou, X. S. Du, Z. Liu, S. P. Ringer and Y. W. Mai, *Synth. Met.*, 2009, **159**, 1302–1307.
93 O. Y. Posudievsky, O. A. Goncharuk and V. D. Pokhodenko, *Synth. Met.*, 2010, **160**, 47–51.
94 C. H. Park, S. K. Jang and F. S. Kim, *Appl. Surf. Sci.*, 2017, **429**, 121–127.
95 X. Wang, Q. Liu, S. Wu, B. Xu and H. Xu, *Adv. Mater.*, 2019, **31**, 1807716.
96 D. Barpuzary, K. Kim and M. J. Park, *ACS Nano*, 2019, **13**, 3953–3963.
97 T. Zhang, H. Qi, Z. Liao, Y. D. Horev, L. A. Panes-ruiz, P. S. Petkov, Z. Zhang, R. Shivhare, P. Zhang, K. Liu, V. Bezugly, S. Liu, Z. Zheng, S. Mannsfeld, T. Heine, G. Cuniberti, H. Haick, E. Zschech, U. Kaiser, R. Dong and X. Feng, *Nat. Commun.*, 2019, **10**(4225), 1–9.
98 S. Majumdar and D. Mahanta, *ChemistrySelect*, 2017, **2**, 9930–9933.
99 L. M. Santino, Y. Diao, H. Yang, Y. Lu, H. Wang, E. Hwang and J. M. D. Arcy, *Nanoscale*, 2019, **11**, 12358–12369.
100 Y. Han, M. Shen, X. Lin, B. Ding, L. Zhang, H. Tong and X. Zhang, *Synth. Met.*, 2012, **162**, 753–758.
101 B. Anothumakkool, R. Soni, S. N. Bhange and S. Kurungot, *Energy Environ. Sci.*, 2015, **8**, 1339–1347.
102 C. S. Inagaki, M. M. Oliveira and A. J. G. Zarbin, *J. Colloid Interface Sci.*, 2018, **516**, 498–510.
103 J. Sui and W. Li, *Soft Mater.*, 2018, **16**, 201–208.
104 Z. Hou, H. Lu, Q. Yang, Q. Zhao and J. Liu, *Electrochim. Acta*, 2018, **265**, 601–608.
105 Y. Wang, K. Cai and X. Yao, *ACS Appl. Mater. Interfaces*, 2011, **3**, 1163–1166.
106 B. H. Yoon, M. Chang and J. Jang, *Adv. Funct. Mater.*, 2007, **17**, 431–436.
107 S. Majumdar, K. Sarmah and D. Mahanta, *ACS Appl. Polym. Mater.*, 2020, **2**, 1933–1942.
108 M. Servalli and A. D. Schl, *Annu. Rev. Mater. Res.*, 2017, **47**, 1–29.
109 G. Qi, Z. Wu and H. Wang, *J. Mater. Chem. C*, 2013, **1**, 7102–7110.
110 S. J. Varma, F. Xavier and S. Jayalekshmi, *Polym. Int.*, 2012, 743–748.
111 D. Yoo, J. Kim and J. H. Kim, *Nano Res.*, 2014, **7**, 717–730.
112 T. Patois, B. Lakard, N. Martin and P. Fievet, *Synth. Met.*, 2010, **160**, 2180–2185.
113 X. Zhang and S. K. Manohar, *J. Am. Chem. Soc.*, 2005, **127**, 14156–14157.
114 Q. Fu, Y. Wang, S. Liang, Q. Liu and C. Yao, *J. Solid State Electrochem.*, 2020, **24**, 533–544.
115 Y. Sun, D. Jia, A. Zhang, J. Tian, Y. Zheng, W. Zhao, L. Cui and J. Liu, *J. Colloid Interface Sci.*, 2019, **557**, 617–627.
116 M. Bharti, P. Jha, A. Singh, A. K. Chauhan, S. Misra, M. Yamazoe, A. K. Debnath, K. Marumoto, K. P. Muthe and D. K. Aswal, *Energy*, 2019, **176**, 853–860.
117 C. Oueiny, S. Berlioz and F. X. Perrin, *Phys. Chem. Chem. Phys.*, 2016, **18**, 3504–3509.